HHS Public Access

Author manuscript

Nat Cancer. Author manuscript; available in PMC 2020 September 01.

Published in final edited form as:

Nat Cancer. 2020 March ; 1(3): 315–328. doi:10.1038/s43018-020-0039-1.

A small-molecule allosteric inhibitor of BAX protects against doxorubicin-induced cardiomyopathy

Dulguun Amgalan[1,2,3], **Thomas P. Garner**[3,4], **Ryan Pekson**[1,3], **Xiaotong F. Jia**[2,3], **Mounica Yanamandala**[1,3,16], **Victor Paulino**[1,3], **Felix G. Liang**[2,3], **J. Jose Corbalan**[1,3], **Jaehoon Lee**[1,3], **Yun Chen**[1,2,3], **George S. Karagiannis**[5,6,7], **Luis Rivera Sanchez**[5,8], **Huizhi Liang**[9], **Swathi-Rao Narayanagari**[2,10], **Kelly Mitchell**[2], **Andrea Lopez**[3,4], **Victoria Margulets**[11,12], **Marco Scarlata**[1,3], **Gaetano Santulli**[1,3,13], **Aarti Asnani**[14,15], **Randall T. Peterson**[14,17], **Rachel B. Hazan**[9,10], **John S. Condeelis**[5,6,7,8,10], **Maja H. Oktay**[5,6,7,9,10], **Ulrich Steidl**[1,2,10], **Lorrie A. Kirshenbaum**[11,12], **Evripidis Gavathiotis**[1,3,4,10,✉], **Richard N. Kitsis**[1,2,3,10,✉]

[1]Department of Medicine, Albert Einstein College of Medicine, Bronx NY, USA.

[2]Department of Cell Biology, Albert Einstein College of Medicine, Bronx, NY, USA.

[3]Wilf Family Cardiovascular Research Institute, Albert Einstein College of Medicine, Bronx, NY, USA.

[4]Department of Biochemistry, Albert Einstein College of Medicine, Bronx, NY, USA.

[5]Department of Anatomy & Structural Biology, Albert Einstein College of Medicine, Bronx, NY, USA.

[6]Gruss-Lipper Biophotonics Center, Albert Einstein College of Medicine, Bronx, NY, USA.

[7]Integrated Imaging Program, Albert Einstein College of Medicine, Bronx, NY, USA.

[8]Department of Surgery, Montefiore Medical Center, Bronx, NY, USA.

[9]Department of Pathology, Albert Einstein College of Medicine, Bronx, NY, USA.

✉**Correspondence and requests for materials** should be addressed to E.G. or R.N.K., evripidis.gavathiotis@einsteinmed.org; richard.kitsis@einsteinmed.org.

Author contributions

R.N.K. and E.G. conceived the research study. D.A. and R.N.K. designed the molecular, cellular and in vivo studies, which were executed by D.A., R.P., X.F.J., M.Y., F.G.L., J.J.C., J.L., Y.C., V.M., M.S., G.S. and L.A.K. E.G. and T.P.G. designed the MST studies, which were executed by T.P.G. E.G., R.N.K., A.L. and D.A. designed the BH3 profiling studies, which were executed by A.L. and D.A. V.P. performed echocardiography. R.N.K., R.B.H. and D.A. designed the LM2 xenograft studies, which were executed by D.A. and H.L. R.N.K, M.H.O., J.S.C. and D.A. designed the breast cancer patient-derived xenograft studies, which were executed by G.S.K., L.R.S. and D.A. R.N.K., U.S., E.G. and D.A. designed the leukemia transplant studies, which were executed by D.A., S.R.N. and K.M. A.A. and R.T.P. designed the zebrafish studies, which were executed by A.A., D.A., E.G. and R.N.K wrote the manuscript with contributions by M.Y. All authors read and approved the final manuscript.

Competing interests

R.N.K., E.G., D.A., T.P.G. and L.A.K. are inventors on a patent application PCT/US2018/021644 submitted by Albert Einstein College of Medicine that covers compounds, compositions and methods for BAX inhibition for the treatment of diseases and disorders.

Additional information

Extended data is available for this paper at https://doi.org/10.1038/s43018-020-0039-1.

Supplementary information is available for this paper at https://doi.org/10.1038/s43018-020-0039-1.

Publisher's note Springer Nature remains neutral with regard to jurisdictional claims in published maps and institutional affiliations.

[10]Albert Einstein Cancer Center, Albert Einstein College of Medicine, Bronx, NY, USA.

[11]Departments of Physiology and Pathophysiology and Pharmacology and Therapeutics, University of Manitoba, Winnipeg, Manitoba, Canada.

[12]Institute of Cardiovascular Sciences, St. Boniface Hospital Albrechtsen Research Centre, Winnipeg, Manitoba, Canada.

[13]Department of Molecular Pharmacology, Albert Einstein College of Medicine, Bronx, NY, USA.

[14]Cardiovascular Research Center, Massachusetts General Hospital, Harvard Medical School, Boston, MA, USA.

[15]CardioVascular Institute, Beth Israel Deaconess Medical Center, Harvard Medical School, Boston, MA, USA.

[16]Present address: Division of Cardiology, Brigham and Women's Hospital, Harvard Medical School, Boston, MA, USA.

[17]Present address: College of Pharmacy, University of Utah, Salt Lake City, UT, USA.

Abstract

Doxorubicin remains an essential component of many cancer regimens, but its use is limited by lethal cardiomyopathy, which has been difficult to target, owing to pleiotropic mechanisms leading to apoptotic and necrotic cardiac cell death. Here we show that BAX is rate-limiting in doxorubicin-induced cardiomyopathy and identify a small-molecule BAX inhibitor that blocks both apoptosis and necrosis to prevent this syndrome. By allosterically inhibiting BAX conformational activation, this compound blocks BAX translocation to mitochondria, thereby abrogating both forms of cell death. When co-administered with doxorubicin, this BAX inhibitor prevents cardiomyopathy in zebrafish and mice. Notably, cardioprotection does not compromise the efficacy of doxorubicin in reducing leukemia or breast cancer burden in vivo, primarily due to increased priming of mitochondrial death mechanisms and higher BAX levels in cancer cells. This study identifies BAX as an actionable target for doxorubicin-induced cardiomyopathy and provides a prototype small-molecule therapeutic.

Essentially all cancer treatment modalities, including traditional chemotherapy, targeted agents and radiation, detrimentally affect the heart with precise toxicities varying with therapy[1]. Heart failure has become a common cause of death among cancer survivors, and the possibility of developing this complication significantly limits the full and effective use of cancer therapeutics[1,2]. The anthracycline doxorubicin remains an essential component in the treatment of solid tumors and leukemias in adults and children. Although its severe, dose-dependent cardiomyopathy has been recognized for almost a half-century[3,4], progress in limiting this cardiotoxicity has been impeded by an incomplete understanding of the underlying mechanism. Doxorubicin kills cancer cells by binding topoisomerase-2, thereby preventing the enzyme from re-ligating the double-stranded DNA breaks that it creates[5]. Some evidence suggests that doxorubicin-induced cardiomyopathy involves the same mechanism[6]. Other data, however, suggest the importance of additional mechanisms including oxidative modifications of proteins and lipids that damage cellular membranes

causing multi-organelle dysfunction[7,8], activation of cytoplasmic proteases[9] and proteotoxic stress[10]. This has made it challenging to identify a single molecular target around which to build a therapy. While cell death is a unifying feature of doxorubicin-induced cardiac damage[2,11,12], even this has proven complex, as it involves a combination of apoptosis and necrosis and it is not clear how one could simultaneously target both of these death programs.

BAX is a member of the BCL-2 family of proteins that resides in an inactive conformation in the cytosol of healthy cells. On cellular stress, BAX undergoes conformational changes that result in its translocation from the cytosol to the outer mitochondrial membrane (OMM) to induce cell death. The key role of BAX in apoptosis is to oligomerize within and permeabilize the OMM allowing release of apoptogens such as cytochrome *c*[13]. In contrast to apoptosis, necrosis in the mitochondrial death pathway is mediated by opening of the permeability transition pore (PTP) in the inner mitochondrial membrane (IMM)[14]. We and others have previously shown that BAX promotes necrosis through its effects on mitochondrial fusion[15] and calcium uptake[16], which sensitize PTP opening. BAX-mediated apoptosis and necrosis are distinct processes, as evidenced by the differential effects of BAX mutants to support one or other of the programs[15,16]. While the conformational requirements of BAX for apoptosis are well defined[17,18], those required for necrosis are less clear.

Because of the dual involvement of apoptosis and necrosis in doxorubicin-induced cardiomyopathy, we hypothesized that BAX may provide a rate-limiting therapeutic target. We present genetic data suggesting that this is the case and delineate the mechanisms by which a small-molecule allosteric inhibitor of BAX blocks apoptotic and necrotic cell death to selectively prevent doxorubicin-induced cardiomyopathy without interfering with cancer treatment.

Results

Doxorubicin-induced cardiomyopathy is dependent on BAX

To test whether BAX is rate-limiting in doxorubicin-induced cardiomyopathy and thus a potential therapeutic target, we subjected male and female wild-type (WT) and BAX knockout (KO) mice (Fig. 1a,b) to a clinically relevant regimen consisting of low doses of doxorubicin over 2 weeks followed by 6–8 weeks observation (Fig. 1c). WT mice treated with doxorubicin weeks earlier manifest systolic dysfunction, as shown by decreased fractional shortening (FS) by echocardiography (Fig. 1d). Reductions in FS were driven by a combination of increased left ventricular end-systolic dimension (LVESD) and decreased left ventricular end-diastolic dimension (LVEDD), the latter reflecting cardiac atrophy, a well-documented feature of this syndrome in humans and mice[19–22]. In contrast, BAX KO mice were protected against doxorubicin-induced systolic dysfunction. Further, WT mice exhibited doxorubicin-induced increases in cardiac apoptosis and necrosis, as assessed by TdT-mediated dUTP nick end labeling (TUNEL) and loss of the chromatin-binding protein HMGB1 (ref. [23]) respectively, which were prevented by the absence of BAX (Fig. 1e,f). These data indicate that doxorubicin-induced cardiomyopathy is dependent on BAX, raising the possibility that BAX may be targeted therapeutically.

Mechanism by which small-molecule BAI1 inhibits BAX in cells

A family of carbazole-based compounds had previously been identified in a screen for small molecules that inhibit cytochrome *c* release from isolated mitochondria stimulated with BID, a member of another class of BCL-2 family proteins, called BH3-only proteins, which bind to and activate BAX and the homologous protein BAK[24,25]. In a companion study, we discovered using nuclear magnetic resonance (NMR) approaches that one such compound, named BAX activation inhibitor 1 (BAI1) (Fig. 2a), binds inactive BAX within a primarily hydrophobic pocket previously uncharacterized and distinct from the trigger site used by the BH3-only proteins to activate BAX[26]. We found that the interaction of BAI1 with this pocket allosterically inhibits BAX conformational activation by stabilizing the hydrophobic core of the protein to maintain the inactive state. Using microscale thermophoresis, we confirmed that BAI1 binds directly to inactive and soluble BAX (Fig. 2b and Extended Data Fig. 1). We next examined the effect of BAI1 on the conformational changes that mediate BAX activation, mitochondrial translocation and insertion into the OMM in cells. An early conformational change induced by the binding of the BH3-only proteins to the BAX trigger site (α-helices 1 and 6) is a shift in the position of the unstructured loop between α-helices 1 and 2 (ref. [17]). This is reflected in the exposure of an epitope in α-helix 1 that is recognized by the 6A7 antibody[27]. BAI1 had no effect on exposure of this epitope in mouse embryonic fibroblasts (MEFs) treated with the apoptosis-inducer staurosporine, indicating that this small molecule does not affect this early conformational change (Fig. 2c). The most critical conformational event in BAX activation, however, is exposure of α-helix 9 containing the transmembrane domain that inserts into the OMM[18]. While antibodies recognizing this domain are lacking due to its hydrophobicity, a surrogate marker is the membrane insertion of BAX. The percentage of BAX that is inserted into the OMM can be assessed by treatment of mitochondria with strong alkali, which is able to extract only loosely attached, but not inserted, BAX[28]. In cells induced to undergo apoptosis, pretreatment with BAI1 reduced the percentage of BAX inserted into the OMM (Fig. 2d). These data indicate that BAI1 blocks staurosporine-induced exposure of α-helix 9, a result corroborated by measurements of solvent access to this helix in cell-free NMR studies[26]. The net result is inhibition of BAX translocation to the mitochondria (Fig. 2e,f). Further, BAI1 blocked BAX-dependent OMM permeabilization and cytochrome *c* release as shown in BAX/BAK-lacking mitochondria reconstituted with truncated BID (tBID)-activated BAX (Fig. 2g). Taken together, our data demonstrate that BAI1 allosterically inhibits the conformational activation of BAX and its subsequent translocation from cytosol to mitochondria.

BAI1 selectively inhibits BAX-dependent apoptosis and necrosis

We next tested the effects of BAI1 on cell death. BAI1 inhibited apoptosis in WT MEFs treated with staurosporine, as evidenced by reductions in apoptotic markers including nuclear fragmentation (Fig. 3a) and externalization of phosphatidylserine (Fig. 3b). Whereas knockout of BAX or BAK in MEFs reduced staurosporine-induced cleaved caspase-3, as expected, treatment with BAI1 resulted in additional protection in BAK KO, but not BAX KO MEFs (Fig. 3c,d). Thus, BAI1 not only binds BAX directly, but BAX is required for it to inhibit apoptosis. Moreover, the presence of BAX is also sufficient for BAI1 to inhibit apoptosis as demonstrated by its protection of BAX/BAK double knockout (DKO) cells reconstituted with BAX alone (Fig. 3e). BAI1 also antagonized necrotic cell death, as shown

by its inhibition of IMM depolarization in WT MEFs treated with the Ca^{2+} ionophore ionomycin for only 1 h (Fig. 3f). Ca^{2+}-induced mitochondrial depolarization at this early time point occurs without cytochrome *c* release, indicative of necrosis[15]. As in the case of apoptosis, BAX was both necessary and sufficient for BAI1 to inhibit necrosis (Fig. 3f).

BAI1 inhibits cardiomyocyte apoptosis and necrosis elicited by diverse stimuli

BAI1 also inhibited apoptotic and necrotic cell death in primary cardiomyocytes. BAX mitochondrial translocation and nuclear fragmentation were attenuated by BAI1 in neonatal rat cardiomyocytes stimulated to undergo apoptosis with staurosporine (Fig. 4a–c). Additionally, loss of plasma membrane integrity, a hallmark feature of necrosis, was blocked by BAI1 even at low nanomolar concentrations in neonatal and adult rat cardiomyocytes subjected to prolonged hypoxia or hypoxia/reoxygenation, which induce primarily necrotic cell death (Fig. 4d,e). Inhibition of necrosis was confirmed by maintenance of IMM potential and reduction in release of HMGB1 (Fig. 4f,g).

Given its ability to inhibit both apoptosis and necrosis, we next tested whether BAI1 could attenuate doxorubicin-induced cardiomyocyte death, which involves both of these death programs. In neonatal rat cardiomyocytes, BAI1 inhibited doxorubicin-induced apoptosis (Fig. 4h). In addition, BAI1 also blocked necrosis as indicated by maintenance of plasma membrane integrity (Fig. 4i,j) and retention of calcein in mitochondria, a readout of PTP closure independent of the IMM potential (Fig. 4k). BAX has been implicated in endoplasmic reticulum Ca^{2+} handling[29,30] and the inositol-requiring enzyme 1α (IRE1α) arm of the endoplasmic reticulum stress response[31]. As these processes may contribute to doxorubicin-induced cell death, we tested whether they were affected by BAI1. We found, however, that BAI1 did not alter baseline or doxorubicin-induced increases in cytosolic or mitochondrial Ca^{2+} concentrations in neonatal rat cardiomyocytes (Extended Data Fig. 2a,b) or doxorubicin-induced activation of IRE1α in MEFs (Extended Data Fig. 2c). Taken together, these data show that BAI1 inhibits apoptotic and necrotic cardiomyocyte death induced by various stimuli.

BAI1 prevents doxorubicin-induced cardiomyopathy

To assess whether BAI1 protects the heart against doxorubicin in vivo, we first employed a well-characterized zebrafish model[32]. BAI1 prevented doxorubicin-induced cardiomyopathy in a dose-dependent manner when the two drugs were administered concurrently (Extended Data Fig. 3). We next tested whether BAI1 could prevent doxorubicin-induced cardiomyopathy in two mouse models. First, we employed the low-dose, long-term doxorubicin model used in the BAX KO studies (Fig. 5a). Because our goal was to test whether BAI1 could prevent doxorubicin-induced cardiomyopathy, the two drugs were administered concurrently every other day, which is also compatible with the 45-h plasma half-life of BAI1 in vivo (Extended Data Fig. 4). BAI1 blocked doxorubicin-induced systolic dysfunction in male and female mice measured 1 month after treatment (Fig. 5b and Extended Data Fig. 5). This was accompanied by prevention of apoptotic and necrotic cardiac cell death (Fig. 5c,d and Extended Data Fig. 5). The second model is an acute doxorubicin model that has traditionally been employed in doxorubicin-induced cardiomyopathy studies, in which a single large dose of doxorubicin is administered

followed by a 5-d observation period. BAI1 prevented cardiac dysfunction in males and females, accompanied by inhibition of apoptotic and necrotic cardiac cell death (Extended Data Fig. 6). Moreover, dosing with BAI1 alone caused no acute or delayed effects on cardiac function or cardiac cell death (Extended Data Fig. 5c–f and Extended Data Fig. 6c) and no mouse mortality (Supplementary Table 1) nor resulted in detectable toxicities in a survey of tissues or blood (Extended Data Figs. 7–9).

BAI1 does not interfere with the chemotherapeutic efficacy of doxorubicin

Doxorubicin is an important component of regimens used to treat breast cancer and leukemia. Accordingly, we tested whether BAI1 attenuates the ability of doxorubicin to treat these malignancies. After confirming that BAI1 treatment alone does not influence cell viability in seven human cancer cell lines (four breast cancer and three acute myeloid leukemia (AML)) (Extended Data Fig. 10a,b), we tested whether this compound interferes with doxorubicin-induced killing of the cells. While nanomolar concentrations of BAI1 protect cardiomyocytes (Fig. 4h–k), concentrations as high as 2.5 μM did not interfere with the ability of doxorubicin to kill cancer cells (Extended Data Fig. 10c,d). Notably, we found that BAI1 does not decrease the ability of doxorubicin to reduce cancer burden in two in vivo models of breast cancer and one of AML. In the first breast cancer model, xenografts of human LM2 cells[33] were created in the mammary fat pad of SCID mice (Fig. 6a). In the second breast cancer model, patient-derived xenografts (PDX) were created using tissue from a woman with triple-negative disease[34,35] (Fig. 6d and Supplementary Table 2a). In both models, the ability of doxorubicin to reduce the volumes and weights of tumors was similar in the presence and absence of BAI1 administered at doses that afford cardioprotection (Fig. 6b,c,e,f).

To assess the effect of BAI1 on the ability of doxorubicin to treat AML, we employed an allograft model in which primary mouse bone-marrow cells, expressing the human MLL-AF9 oncogene were injected into the bloodstream of sublethally irradiated immunocompetent mice[36,37] (Fig. 6g). An allograft model was chosen for these studies so that the effects of BAI1 on doxorubicin-induced cardiomyopathy could be assessed in the same mice undergoing treatment for AML. This is not possible in the immunodeficient mice used in the xenograft models because, when treated with doxorubicin, these mice do not survive long enough to develop cardiomyopathy. As in the breast cancer models, BAI1 did not interfere with the ability of doxorubicin to reduce bone-marrow leukemic infiltration (Fig. 6h). Notably, BAI1 also rescued cardiomyopathy in these same animals (Fig. 6i). These data show that BAI1 can prevent cardiomyopathy without compromising the efficacy of doxorubicin to limit cancer burden.

Mechanism for the selectivity of BAI1 in protecting the heart without compromising cancer treatment

We next considered the mechanism by which BAI1 selectively protects the heart against doxorubicin without interfering with the killing of cancer cells. RNA-sequencing data from large numbers of individuals show that BAX expression is lowest in the heart compared to other organs and highest in transformed cells (Fig. 7a). Consistently with this, we found that BAX expression is highly upregulated in cancers, including in breast cancer and AML,

compared to healthy controls (Fig. 7b). Further, in addition to the expected increases in the expression of anti-cell death BCL-2 members in cancers[38], we found that BAX mRNA and protein levels are also markedly higher in breast cancers derived from our PDX model and human cancer cell lines than in adult mouse, rat and human hearts (Fig. 7c,d and Supplementary Table 2). On the basis of these data, we hypothesized that the higher BAX levels in cancers compared to heart contribute to the inability of BAI1 to inhibit doxorubicin-induced killing of cancer cells. To test this, we first assessed the relative sensitivities of mitochondrial death mechanisms in cancer cells versus cardiomyocytes using BH3 profiling[39,40]. Cells isolated from PDX tumors and adult mouse heart tissues were permeabilized and treated with peptides containing the BH3 helices of BID or BIM. While mitochondrial cytochrome *c* release occurred readily and in a dose-dependent manner in PDX-derived tumor cells, cardiac cells were completely resistant (Fig. 7e). Similar results were obtained with BH3 profiling of human cancer cells versus neonatal rat cardiomyocytes, using mitochondrial depolarization as the readout (Fig. 7f). These data show that mitochondrial death mechanisms in cancer cells are significantly more primed than in cardiomyocytes. As these observations were made under basal conditions, we next assessed the effect of doxorubicin treatment on priming. BH3-induced mitochondrial depolarization was sensitized by doxorubicin in both cancer cells and cardiomyocytes. However, while BAI1 blunted depolarization in cardiomyocytes, it failed to do so in cancer cells (Fig. 7g). To test whether high BAX levels contribute to the ineffectiveness of BAI1 to inhibit doxorubicin-induced killing of cancer cells, we knocked down BAX abundance ~73% in THP-1 AML cells (Fig. 7h). Depletion of BAX rendered doxorubicin-induced killing of these cells susceptible to inhibition by BAI1 (Fig. 7h). These data demonstrate that the higher levels of BAX in cancer cells contribute to the inability of BAI1 to inhibit their killing by doxorubicin.

Discussion

Previous studies have reported small molecules that inhibit BAX-mediated apoptosis[41–43]. However, the mechanisms by which these work remain poorly defined. None have been shown to bind BAX directly. Some likely work through nonspecific effects on mitochondrial membrane function, whereas others interfere with BAX oligomerization, an event required for apoptosis but not necrosis[15,16]. Accordingly, these small molecules are not strong candidates for a drug to inhibit both apoptotic and necrotic cell death. In contrast, BAI1 binds directly to BAX in a new regulatory pocket to allosterically inhibit the conformational activation of this protein and its translocation to mitochondria, thereby abrogating both of these cell death programs.

Multiple pathophysiological processes have been implicated in doxorubicin-induced cardiomyopathy and this complexity has impeded identification of a truly rate-limiting therapeutic target. Our data employing both genetic and chemical approaches demonstrate that BAX is a convergence point for these mechanisms and confirm that both apoptotic and necrotic myocardial cell death are critical in the pathogenesis of doxorubicin-induced cardiomyopathy. While cell death is important, doxorubicin also directly damages multiple cellular components, causing organelle dysfunction. We hypothesize that inhibition of cell

death provides a temporal window within which endogenous cellular repair mechanisms attenuate direct damage from doxorubicin.

The ability of BAI1 to inhibit cardiac cell death without interfering with cancer cell killing is somewhat unexpected. We believe that this reflects the increased priming of mitochondrial death mechanisms in cancer cells compared to cardiomyocytes. This result is consistent with previous work comparing the threshold for cell death activation in proliferating versus terminally differentiated cells[40]. Our knockdown studies reveal that the considerably higher BAX levels in most, if not all, cancer cells contribute to the inability of BAI1 to inhibit doxorubicin-induced killing. BAX levels and BH3 profiling of cancer biopsies[39] could potentially be combined with clinical risk factors[44] and genetic markers[45] for doxorubicin-induced cardiomyopathy in deciding whether to employ BAI1 for cardioprotection. As BAX levels in most cancers seem to dwarf those in the heart, it is possible that BAI1 may be widely applicable. Moreover, in addition to high BAX levels, it is likely that cancer cell killing escapes inhibition by BAI1 due to other factors (for example BAK) that prime mitochondrial death mechanisms.

Our delineation of the structural basis for the BAI1–BAX interaction[26] and the conformational changes by which BAI1 modulates BAX function in cells herein provide the opportunity for the rational optimization of this compound. BAX inhibitors based on this prototype may afford a means not only to prevent doxorubicin-induced cardiomyopathy, but also to allow this chemotherapeutic to be deployed at higher doses and in combination with other cardiotoxic drugs to more effectively treat cancer. In addition, while it remains to be tested, cardiomyopathies resulting from other cancer therapies may also be BAX-dependent and ameliorated by BAI1. For example, MEK1 inhibitors activate BAX in cancer cells by inhibiting the phosphorylation and subsequent proteasomal degradation of BIM[46,47]. Moreover, as the first dual inhibitor of mitochondrial-mediated apoptosis and necrosis, BAI1 may provide a means to reduce tissue damage in other syndromes, such as myocardial infarction and stroke, in which both of these cell death programs operate.

Methods

Animal studies

All animals were housed under conditions outlined in the National Institutes of Health Guide for Care and Use of Laboratory Animals in compliance with the US Department of Agriculture Laboratory Animal Welfare Act. Mice and neonatal rat experiments were approved by the Institutional Animal Care and Use Committee of the Albert Einstein College of Medicine. Adult rat experiments were approved by the Institutional Animal Care and Use Committee of the University of Manitoba. Zebrafish experiments were approved by the Institutional Animal Care and Use Committees of Massachusetts General Hospital and Beth Israel Deaconess Medical Center.

Genotyping of BAX KO mice

PCR of genomic DNA was used to genotype progeny of *Bax*$^{+/-}$ breedings. The primers were as follows: primer 1: 5’-GTTGACCAGAGTGGCGTAGG-3’; primer 2: 5’-

CCGCTTCCATTFCTCAGCGG-3'; and primer 3: 5'-GAGCTGATCAGAACCATCATG-3'. The conditions are as described (www.jax.org/strain/002994). Primers 1 and 3 identify the $Bax^{+/+}$ allele; primers 1 and 2 identify the $Bax^{-/-}$ allele.

Preparation of primary cultures of cardiomyocytes

Neonatal rat cardiomyocytes (NRCMs) were isolated from 1–2-day-old Sprague-Dawley rats as previously described[48]. NRCMs were cultured for 2 d before treatments. Adult rat cardiomyocytes were isolated from male Sprague-Dawley rats (250–300 g) as previously described[49].

Production of recombinant BAX protein

Recombinant human BAX protein was expressed in *Escherichia coli* and monomers were purified using size-exclusion chromatography as previously described[50,51].

BAX activation inhibitor 1

BAI1 was purchased (Millipore, 196805) or synthesized by the Chemical Synthesis Core Facility of the Albert Einstein College of Medicine. For both, the identity and purity (>98%) was confirmed by NMR and mass spectrometry analysis. For all cell culture experiments, BAI1 was pretreated for 1 h before addition of stress inducers.

Microscale thermophoresis

Recombinant BAX protein was labeled at 1 or 2 cysteines using the Monolith Protein Labeling Kit RED-MALEIMIDE (NanoTemper Technologies) according to the manufacturer's instructions. To determine the K_d of BAI1-BAX binding, 100 nM of labeled BAX was incubated with increasing concentrations of BAI1 for 10 min at room temperature and microscale thermophoresis (MST) was measured using Monolith NT.115 Blue/Red (NanoTemper Technologies). Binding data were analyzed using the temperature jump region (1.6 s) of the MST curves and fitted using GraphPad Prism (GraphPad Software). Similar results were obtained with BAX labeled with 1 or 2 dye molecules per BAX molecule.

Assessment of early events in BAX conformational activation

MEFs were treated with 2 μM STS for 4 h. Cell lysates were subjected to immunoprecipitation using Dynabead (Invitrogen, 10004D)-conjugated BAX 6A7 antibody, which recognizes an epitope in α-helix 1 exposed early following BH3-only protein binding to BAX[27]. Dynabead-conjugated mouse IgG was used as a control. After recovery of immunoprecipitated proteins from Dynabeads, western blot was performed using an antibody that recognizes total BAX and band intensity quantified (LI-COR, ImageStudio).

Assessment of late events in BAX conformational activation

OMM insertion was employed as a marker of BAX α-helix 9 exposure. MEFs were treated with 2 μM STS for 4 h. BAX insertion was assessed using alkali treatment of isolated mitochondria that recovers only loosely attached, noninserted BAX[28]. Cell lysates were centrifuged at 10,000*g* for 10 min and the mitochondrial fraction recovered in the pellet. Isolated mitochondria were incubated with 0.1 M Na_2CO_3 (pH 10.5) for 20 min on ice or

with an equal volume of water as a negative control. Supernatant and mitochondria were separated by centrifugation at 20,000*g* for 30 min. These fractions were analyzed by western blot for BAX and COX4. Inserted BAX was calculated as ((total – noninserted)/total) × 100%.

BAX mitochondrial translocation

BAX translocation was quantified in MEFs and NRCMs by the presence of mitochondrial-localized BAX puncta as previously described[52]. Cells were treated with 2 μM STS for 3 h (MEFs) or 5 h (NRCMs). For MEFs, mitochondria were identified using MitoTracker Red (Invitrogen, M22425) before fixation according to the manufacturer's protocol. Cells were fixed in 4% paraformaldehyde, permeabilized in PBS with 0.5% Triton X-100 and blocked with PBS with 2% BSA and 1% Triton X-100. Immunostaining was performed using BAX antibody and Alexa Fluor 488 secondary antibody. For NRCMs, mitochondria were identified by co-immunostaining with ATP5α antibody and Alexa Fluor 546 secondary antibody. After counterstaining of nuclei with either Hoechst 33342 or DAPI (Vector Laboratories, H-1500) slides were visualized using Axio Observer.Z1 microscope (Carl Zeiss) at ×200 magnification. Five fields per treatment (~250–350 cells per field) were randomly selected and the percentage of cells with mitochondrial BAX puncta was scored.

Cytochrome *c* release from isolated mitochondria

Isolated mitochondria (40 μg) from BAX/BAK DKO MEFs were incubated with 25 nM recombinant human BAX, 10 nM recombinant human tBID (R&D Systems, 882-b8–050) with or without 10 μM BAI1 at 37 °C. After 50 min, mitochondria were centrifuged at 8,000*g* and cytochrome *c* was assessed in the mitochondrial pellet using Quantikine cytochrome *c* immunoassay (R&D, MCTC0) according to the manufacturer's protocol.

Cleaved caspase-3 by immunofluorescence in cells

Cleaved caspase-3 was assessed in MEFs treated with 2 μM STS for 4 h. Following fixation and permeabilization, immunostaining was performed using cleaved caspase-3 antibody and Alexa Fluor 546 secondary antibody. Slides were visualized using Axio Observer.Z1 microscope at ×100 magnification. Five fields per treatment (~500 cells per field) were randomly selected and the percentage of cells with cleaved caspase-3 was scored.

Nuclear fragmentation assay

MEFs were treated with 2 μM STS for 3 h. Following fixation and permeabilization, nuclei were stained with Hoechst 33342 or DAPI and visualized using Axio Observer.Z1 microscope at ×200 magnification. Five fields per treatment (~250–350 cells per field) were randomly selected and the percentage of cells with fragmented nuclei was scored. NRCMs were treated with 2 μM STS for 5 h or 1 μM DOX for 6 h. Slides were visualized at ×200 magnification (STS) or ×100 magnification (DOX). Five fields per treatment for STS (~100 cells per field) or three fields per treatment for DOX (~700 cells per field) were randomly selected.

Annexin V staining

Externalization of phosphatidylserine was assessed by annexin V binding in MEFs treated with 2 μM STS for 4 h using the Dead Cell Apoptosis kit with annexin V Alexa Fluor 488 (Invitrogen, V13241) per the manufacturer's protocols. Percentage of cells positive for annexin V staining was quantified using FlowJo software (Tree Star).

Loss of mitochondrial membrane potential

MEFs were treated with 10 μM ionomycin for 30 min. Unfixed cells were then incubated with 2 μM TMRE (Invitrogen, T669) for 15 min at 37 °C in the dark, trypsinized and resuspended, and fluorescence was analyzed with an LSRII flow cytometer (BD Biosciences). The percentage of cells that lost TMRE fluorescence was quantified using FlowJo software. NRCMs were subjected to hypoxia for 18 h in a chamber infused with 95% nitrogen and 5% carbon dioxide at 37 °C as described[53]. Composition of the air was confirmed by oxygen sensor/controller (Biospherix, ProOx Model 110). Following staining with TMRE as above, cells were visualized with an Olympus AX-70 microscope at ×400 magnification. Five fields per treatment (~40 cells per field) were randomly selected and the relative TMRE fluorescence was quantified per cell using ImageJ. TMRE fluorescence in the control was assigned a mean value of 1 and the other conditions were expressed relative to this.

Mitochondrial calcein-AM retention

NRCMs were treated with 5 μM DOX for 18 h. Cells were incubated with 5 μM calcein-AM (Invitrogen, C3100MP) for 30 min in the presence of 2 mM $CoCl_2$ at 37 °C. Cells were visualized with an Olympus AX-70 microscope at ×400 magnification. Five fields per treatment (~40 cells per field) were randomly selected and relative calcein fluorescence was quantified per cell using ImageJ. Calcein fluorescence in the control was assigned a mean value of 1 and the other conditions were expressed relative to this.

Entry of ethidium homodimer into cells

NRCMs were subjected to hypoxia or 5 μM DOX for 18 h. Adult rat cardiomyocytes were subjected to hypoxia for 1 h followed by 2 h of reoxygenation. Cells were stained with Live/Dead Viability/Cytotoxicity kit (ThermoFisher, L3224), which contains 2 μM calcein-AM and 2 μM EthD. Cells were visualized with an Olympus AX-70 microscope at ×400 magnification. Five fields per treatment (~40 cells per field) were randomly selected and the percentage of cells with EthD fluorescence was quantified.

LDH release from cells

NRCMs were treated with 5 μM DOX for 18 h. Relative LDH activity in the medium was measured with In Vitro Toxicology assay kit (Sigma, TOX7) using a microplate reader (BioRad, iMark).

HMGB1 release from cells

NRCMs were subjected to hypoxia for 18 h. Equal volumes of medium per treatment were analyzed by western blot for HMGB1. As these cells were cultured in serum-free medium, a loading control could not be performed.

Mitochondrial calcium handling

NRCMs were treated with DOX for 1 h. Mitochondrial Ca^{2+} fluxes were evaluated as previously described[54,55]. Briefly, cells were loaded with 3 μM Rhod-2 acetoxymethyl ester for 30 min at 37 °C followed by washout and 1 h rest at 20 °C for de-esterification. Fluorescence was detected using a pass-band filter of 545–625 nm in response to excitation at 542 nm. Cytosolic Ca^{2+} was measured via ratiometric (F650/F515) imaging of Fluo-4 (excited at 488 nm and emission collected at 505–530 nm) and Fura Red (excited at 488 nm and emission collected at >650 nm), as described[56–58]. Live cell imaging was performed using LSM 5 Live confocal microscope (Carl Zeiss) at ×630 magnification. Images and data were processed and analyzed using Fiji Software9.

Zebrafish model of doxorubicin-induced cardiomyopathy

TuAB zebrafish embryos at 30 h post-fertilization in 96-well plates were treated with 100 μM DOX (Sigma, D1515) as previously described[32] (n = 6 fish per group were studied). Cardiomyopathy was scored on the basis of decreased cardiac contraction, pericardial edema and decreased tail blood flow as assessed by light microscopy at ×50 magnification 40 h post-treatment. Protection was defined as the absence of all three of these phenotypes.

Pharmacokinetic analysis

Adult WT C57BL/6J male mice were administered BAI1 at 1 mg kg^{-1} by a single intravenous bolus injection via the tail vein and blood sampling was performed at 15 min, 30 min, 1 h, 2 h, 4 h, 8 h and 24 h. Because repeated blood sampling from a mouse may alter physiology, individual mice were studied at each time point (n = 3 mice per time point). Plasma BAI1 concentrations were determined using a triple quadrupole LC–MS/MS assay. Pharmacokinetic parameters were calculated using Phoenix WinNonlin by a noncompartmental model.

Mouse models of doxorubicin-induced cardiomyopathy

General information—Numbers, age and sex of mice are specified in figure legends of each experiment. All mice were analyzed by echocardiography. For all subset analyses, tissues were randomly chosen. Mortality data for every mouse used in cardiac studies are shown in Supplementary Table 1.

Long-term model—DOX (Tocris Bioscience, 2252) at 3 mg kg^{-1} dissolved in saline was administered intraperitoneally (i.p.) (4 μl g^{-1}) to male and female C57BL/6J mice every other day for 2 weeks (total eight doses). Control mice received the same volume of saline. In pilot experiments, echocardiography demonstrated decreases in systolic function at 6 weeks following initiation of DOX (earliest time point examined) and persisting to 12 weeks

(latest time point examined). Accordingly, in our full experiments, we performed echocardiography 6–10 weeks after initiation of therapy.

Acute model—DOX at 20 mg kg^{-1} dissolved in saline was administered i.p. (4 μl g^{-1}) one time to male and female C57BL/6N mice. Control mice received the same volume of saline. To prevent dehydration from decreased fluid intake, all mice were i.p. injected with 500 μl of saline per day for 5 d starting the day after DOX administration. Mice underwent echocardiography 5 d after treatment.

BAI1 treatment of mice

BAI1 at 71.9 mM dissolved in 100% DMSO was diluted 100-fold into 20% PEG-400 (Qiagen, 133086) and 80% D5W (dextrose 5% in water). The final solution consisted of 0.719 mM BAI1 in 1% DMSO (v/v), 19.8% PEG-400 (v/v) and 79.2% D5W (v/v) (this solvent is referred to as vehicle). BAI1 at 2 mg kg^{-1} in vehicle was administered i.p. (4 μl g^{-1}) at the same time as DOX or saline control (injected into contralateral sides). Accordingly, the randomly assigned treatment groups consisted of: (1) saline + vehicle (saline); (2) saline + BAI1 (in some experiments as indicated) (BAI1); (3) DOX + vehicle (DOX); and (4) DOX + BAI1.

Echocardiography

Echocardiography was performed under isoflurane anesthesia on a 37 °C heated platform using a Vevo 2100 ultra-high frequency imaging system with a MS550D mouse transducer (VisualSonics). Left ventricular internal dimensions were measured in end-diastole (LVEDD) and end-systole (LVESD) in the short-axis view for three continuous cardiac cycles and averaged. Left ventricular FS and LVEDD-LVESD were calculated from these measurements[59,60].

TUNEL on cardiac tissue

Paraffin sections (5 μm) of mouse hearts fixed in 10% phosphate-buffered formalin were analyzed by TUNEL (Promega, G3250) according to manufacturer's recommendations. After mounting with DAPI, slides were examined using Axio Observer.Z1 microscope at ×200 magnification. Five fields (>400 cells per field) were randomly selected for analysis.

Cleaved caspase-3 immunohistochemistry of cardiac tissue

Paraffin-embedded mouse heart sections were deparaffinized and antigen retrieval was performed by boiling in citrate buffer. Following inactivation of endogenous peroxidase and blocking in 5% goat serum and 2% BSA, sections were incubated with cleaved caspase-3 antibody, followed by biotinylated secondary antibody. Sections were incubated with ABC-HRP (Vector Laboratories, PK-6100) and 3,30-diaminobenzidine tetrahydrochloride. Slides were imaged using the PerkinElmer P250 High Capacity Slide Scanner at ×200 magnification and densitometry of immunohistochemistry analyzed using the 'Densito Quant Module' (3DHISTECH), which measures a positive signal based on RGB values. Percentage of myocardial cross-sectional area positive for cleaved caspase-3 signal was determined.

HMGB1 immunofluorescence on cardiac tissue

Paraffin-embedded mouse heart sections were deparaffinized and antigen retrieval was performed using antigen unmasking solution (Vector Laboratories, H-3300). Following blocking in 10% goat serum and 0.01% Triton X-100, sections were incubated with HMGB1 primary antibody, followed by Alexa Fluor 488 secondary antibody. Slides were examined using Axio Observer.Z1 microscope under ×400 magnification. Three to four fields (>200 cells per field) were randomly selected for analysis. Staining was interpreted as follows: aqua color (green HMGB1 + blue DAPI) indicated presence of HMGB1; blue color (DAPI alone) indicated loss of HMGB1.

LM2 human breast cancer xenograft mouse model

Human breast cancer cells MDA-MB-231-LM2–4175 (ref. [33]) (referred to as LM2 cells), suspended at 1×10^6 cells in 100 μl of PBS, were injected into the right inferior mammary fat pad of 8-week-old female SCID mice under isoflurane anesthesia[61]. Tumor volume, calculated as $0.5 \times (\text{long axis}) \times (\text{short axis})^2$, was measured twice a week using calipers. Once tumors reached 50–100 mm^3, mice were randomly assigned to treatment groups ($n = 5$ mice per group) such that each group had similar mean tumor volumes at the time of randomization. Treatments were administered i.p. to contralateral sides of the abdomen 30 and 34 d after injection of cells. On day 38, tumor volumes were measured, mice were killed and tumors were weighed.

Breast cancer patient-derived xenograft mouse model

De-identified breast cancer patient tissue samples obtained with the approval of the Institutional Review Board of the Albert Einstein College of Medicine and Montefiore Medical Center were provided by J.S. Condeelis and M. Oktay of these institutions. The development of the PDX model has been described previously[34,35] and the clinical characteristics of the patient shown in Supplementary Table 2. A 1-mm^3 tumor chunk was transplanted orthotopically in the right fourth mammary fat pad of 8-week-old female SCID mice under isoflurane anesthesia. Following ~4 weeks to allow tumor growth, mice were randomly assigned to treatment groups ($n = 9$–11 mice per group) such that the mean tumor volume of each group at the time of randomization was ~50 mm^3. Treatments were administered i.p. to contralateral sides of the abdomen 25 and 32 d after transplantation of tumor. On day 35, tumor volumes were measured, mice were killed and tumors were weighed.

Human MLL-AF9 AML allograft mouse model

Bone marrow was isolated from WT C57BL/6J mice (CD45.2). $Lin^-Kit^+Sca\text{-}1^+$ cells were separated by FACS and cultured. Then, cells were transduced with MSCV-MLL-AF9-IRES-GFP retrovirus and plated in methylcellulose (R&D Systems, HSC007) for 5 d (refs. [36,37,62]). GFP-positive cells were FACS sorted and 1.2×10^5 cells were retro-orbitally transplanted into a sublethally irradiated (650 rads) congenic C57BL/6 mouse (CD45.1) to generate an MLL-AF9 leukemic primary recipient mouse. For secondary transplantation, liver was isolated from the leukemic primary recipient mouse and GFP-positive cells were sorted by FACS. A total of 5,000 cells were injected retro-orbitally on day 1 into 8-week-old

male congenic C57BL/6 (CD45.1) secondary recipient mice that had received sublethal irradiation (250 rads) on day 0. Mice were randomly assigned to treatment groups (n = 10 mice per group). Starting on day 12, treatments were administered i.p. to contralateral sides of the abdomen every other day for a total of ten doses. At 19, 26 and 33 d after injection of cells, bone marrow was aspirated to analyze leukemic infiltrates as described below. On day 34, echocardiography was performed followed by killing.

Analysis of leukemic infiltrates in bone marrow

Chimerism analysis was performed on cells aspirated from femurs. Bone-marrow aspirates were treated with ammonium chloride potassium solution to lyse erythrocytes and remaining cells were resuspended in PBS with 2 mM EDTA. To distinguish donors from host cells in transplanted mice, cells were stained with phycoerythrin (PE)-conjugated host CD45.1 antibody and allophycocyanin (APC)-conjugated donor CD45.2 antibody. DAPI at 10 μg ml $^{-1}$ was added to mark dead cells before analysis by LSRII flow cytometer. After cells were selected in the forward versus side scatter (FSC/SSC) dot plot to remove debris, they were gated to exclude cellular aggregates in the FSC/FSC and FSC/SSC dot plots. Gates of PE^+, APC^+ and GFP^+ cells were set and compared to a control sample with no detectable fluorochrome expression. Data were analyzed using FlowJo software.

BAX expression in human databases

BAX transcript levels as determined by RNA sequencing in various human tissues were obtained from the Genotype-Tissue Expression database (n = 111–473). Data on n = 778 breast tumor and n = 100 control samples were obtained from the Breast Cancer Cohort of The Cancer Genome Atlas. Data on n = 542 AML and n = 74 control samples were obtained from the Microarray Innovations in LEukemia study (GEO database, GSE13204).

BAX mRNA copy numbers in human hearts and cancers

De-identified normal human heart samples obtained with the approval of the Institutional Review Board of the University of Pennsylvania and of Albert Einstein College of Medicine were provided by K.B. Margulies and K. Bedi of the University of Pennsylvania. Characteristics of the donors from whom heart samples were derived are shown in Supplementary Table 2. Briefly, the four heart tissue samples comprised two female and two male donors between 47 and 63 years old. Human heart samples, cancers from the PDX model, human breast cancer cell lines (LM2, MCF-7, MDA-MB-231, 3475) and human AML cell lines (THP-1, MOLM-13, HL-60) were prepared for total RNA extraction using Trizol Reagent (ThermoFisher, 15596018). Total RNA was then reverse transcribed to cDNA using SuperScript III First-Strand Synthesis System (ThermoFisher, 18080–051). To compare absolute copy numbers of BAX transcripts across different tissues and cells with quantitative real-time RT-PCR, a standard curve was developed using known copy numbers of human BAX cDNA in pcDNA 3.1 vector: 100,000, 10,000, 1,000, 500, 100, 50, 20 and 10 copies. Real-time PCR was performed with a Taqman probe for BAX (ThermoFisher, Hs00180269_m1) using ViiA 7 Real-Time PCR System (Applied Biosystems). Standards and samples were assayed in triplicates. A linear standard curve was constructed with copy number of the standard plasmid DNA versus the threshold cycle (R^2 = 0.9976) and used to calculate the absolute BAX mRNA copy numbers in the samples.

Cancer cell viability assay

To assess whether BAI1 alone affects the viability of cancer cells, human breast cancer and human AML cell lines were treated with BAI1 for 24 h. Cell viability was assessed using CytoTox-Glo cytotoxicity assay (Promega, G9291). Luminescence was detected by a microplate reader (TECAN, F200 PRO). To assess whether BAI1 influences the effect of DOX, cancer cells were pretreated with BAI1 for 1 h followed by treatment with doxorubicin for 24 h. The following doxorubicin concentrations were used: 1 μM for LM2; 2 μM for MDA-MB-231 and 3475; 8 μM for MCF-7; 400 nM for THP-1, MOLM-13 and HL-60. Cells receiving no DOX and no BAI1 were assigned a viability of 100% (not shown on graphs).

Intracellular BH3 profiling of PDX cancers versus heart tissue

Cancer tissues from the PDX model were compared to heart tissues from adult WT C57BL/6J mice using intracellular BH3 profiling[63]. Tissue samples were digested in DMEM with liberase (50 μg ml^{-1} DL (Sigma, 5466202001) and 50 μg ml^{-1} TL (Sigma, 05401020001)) at 37 °C for 20 min to dissociate cells for flow cytometry. Cells were then resuspended in MEB buffer and 200,000 cells were used per condition. Cells were treated with BH3 peptides, BID and BIM (0.1 μM, 1 μM, 10 μM and 100 μM) and PUMA2A (100 μM) in MEB buffer with 0.001% (w/v) digitonin. PUMA2A and DMSO treatments served as negative controls that retain mitochondrial cytochrome *c*. Cells were then stained with Alexa Fluor 488 anti-cytochrome *c* antibody or Alexa Fluor 488 mouse IgG1 isotype control antibody and analyzed with LSRII flow cytometer to measure mitochondrial cytochrome *c* retention. Gates were drawn in a scatter-plot consisting of side scatter (SSC) versus cytochrome *c* using isotype control as a guide for negative staining. Peptide sequences for BH3 peptides are as follows: BID, acetyl-EDIIRNIARHLAQVGDSMDRY-amide; BIM, acetyl-MRPEIWIAQELRRIGDEFNA-amide; PUMA2A, acetyl-EQWAREIGAQARRMAADLNA-amide.

BH3 profiling of cancer cell lines versus NRCMs

Human breast cancer and AML cell lines were compared to NRCMs using BH3 profiling[39,64]. This was performed under basal conditions as well as following treatment of cells with DOX. In the latter case, effects of BAI1 were also assessed. A total of 2×10^4 MDA-MB-231, 2×10^4 LM2, 4×10^4 MOLM-13 and 1×10^4 NRCMs per well were plated in 384-well plates. Following cellular permeabilization, BIM BH3 peptide was added and mitochondrial depolarization was assessed with JC-1 using a microplate reader (TECAN, M1000). For basal studies, BIM BH3 peptide was used at a concentration of 10 μM for cancer cells and 10 μM or 100 μM for NRCMs. For the studies employing combinations of doxorubicin and BAI1, BIM BH3 peptide was applied at 0.5 μM, 1 μM and 0.1 μM for MDA-MB-231, MOLM-13 and NRCMs respectively. BAI1 was added to cells at a concentration of 0.15 μM for 1 h before doxorubicin. DOX was applied for 23 h at concentrations of 0.5 μM, 0.15 μM and 1.5 μM for MDA-MB-231, MOLM-13 and NRCMs respectively.

BAX siRNA silencing

THP-1 cells were electroporated with 200 nM siControl (Life Technologies, 4390846) or siBAX (Life Technologies, 4390824) using Amaxa Cell Line Nucleofector kit V per the manufacturer's protocol (Lonza, VCA-1003). The effect of BAI1 on DOX-induced killing was assessed 24 h after nucleofection. Following pretreatment with BAI1 for 1 h, cells were treated with 200 nM DOX for 24 h and cell death was assessed using a Caspase-Glo 3/7 assay (Promega, G6320).

Toxicity studies in vivo

Vehicle or BAI1 at 2 mg kg^{-1} was administered i.p. (~4 μl g^{-1}) every other day for 2 weeks (total eight doses) to 12-week-old female C57BL/6J mice. At week 6 after initiation of BAI1, peripheral blood was obtained from the tail vein. Blood counts were determined by Genesis Blood Analyzer (Oxford Sciences). Mice were then killed and tissues (heart, lung, kidney, liver, spleen, tibia and brain) were collected and fixed in 10% formalin. Paraffin-embedded sections were stained with hematoxylin and eosin and examined.

Statistics and reproducibility

Sample size calculations for the long-term and acute DOX models were based on the effects on FS observed in pilot experiments. Sample size calculations for the breast cancer PDX model were based on data from the LM2 breast cancer xenograft model. Power calculations were performed via bootstrap sampling to ensure that the null hypothesis would be correctly rejected with >80% power at the 0.05 significance level. The power analyses indicated that the following sample sizes were required: long-term DOX model, $n = 6$; acute DOX model, $n = 5$; PDX model, $n = 9$. No data were excluded from the analyses. For in vivo breast cancer studies, tumor-bearing mice were assigned to treatment groups, such that the mean tumor volume was similar among groups at the start of treatment. In all other in vivo experiments, animals were randomly assigned into experimental groups. In experiments in which pretreatment echocardiograms were performed, the randomly assigned treatment groups had similar starting mean FS values. For all subset analysis, tissues were randomly chosen. For microscopic images, fields were randomly selected for analyses. The echocardiographer was blinded to the genotypes/treatment groups throughout the performance and analysis of the studies. Other investigators were not blinded to allocation during experiments and outcome assessment. Statistical comparisons were performed using one-way ANOVA with Tukey's multiple comparisons test correction when three or more groups were compared. A two-tailed Student's *t*-test or two-sided Wilcoxon rank-sum test was used to compare two groups. *P* values and *n* values are indicated in figures or figure legends. Plots and statistical tests were carried out using GraphPad Prism 7 (GraphPad Software) and Statsmodels and scipy.stats (Python packages).

Reporting Summary

Further information on research design is available in the Nature Research Reporting Summary linked to this article.

Data availability

Source data for all figures are provided with the paper online. All other data supporting the findings of this study are available from the corresponding authors upon reasonable request.

Code availability

Details and code for the power analyses can be found in the GitHub repository (https://github.com/celldeath/power_analysis).

Extended Data

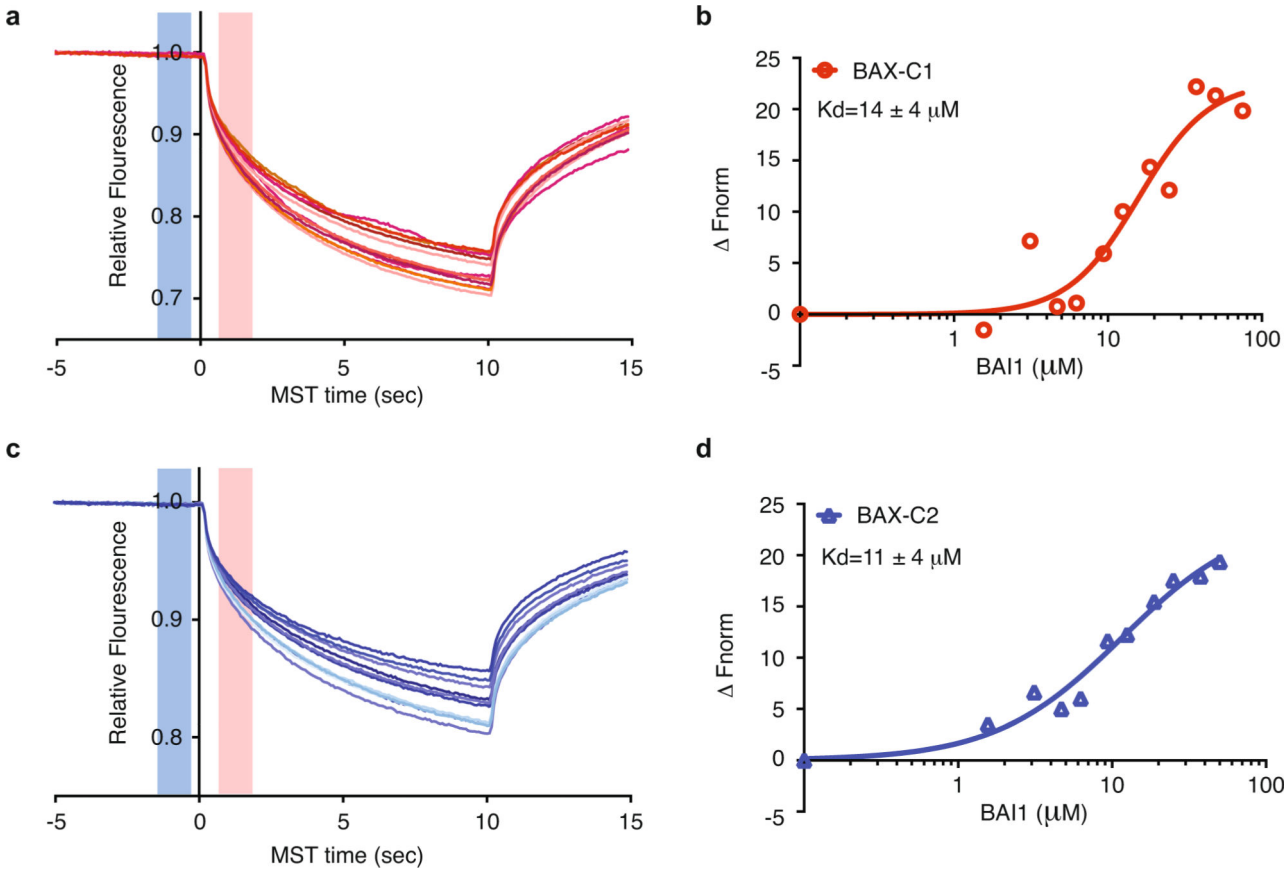

Extended Data Fig. 1 |. BAI1 binding to BAX as assessed by microscale thermophoresis (MST). Relates to Fig. 2b. **a**, **c**, Examples of MST which measures the thermophoretic movement induced by infrared laser activation of labeled BAX as reflected by relative fluorescence as a function of time. Cold start region indicated by blue box. Warm region indicated by pink box. Each curve denotes a different concentration of BAI1. BAX was labeled with 1 (C1, red curves) or 2 (C2, blue curves) dye molecules/BAX molecule yielding similar results. Representative of 3 independent experiments. **b**, **d**, Binding curves determined using the temperature jump region of the curve (pink box) normalized to the cold start region (blue box).

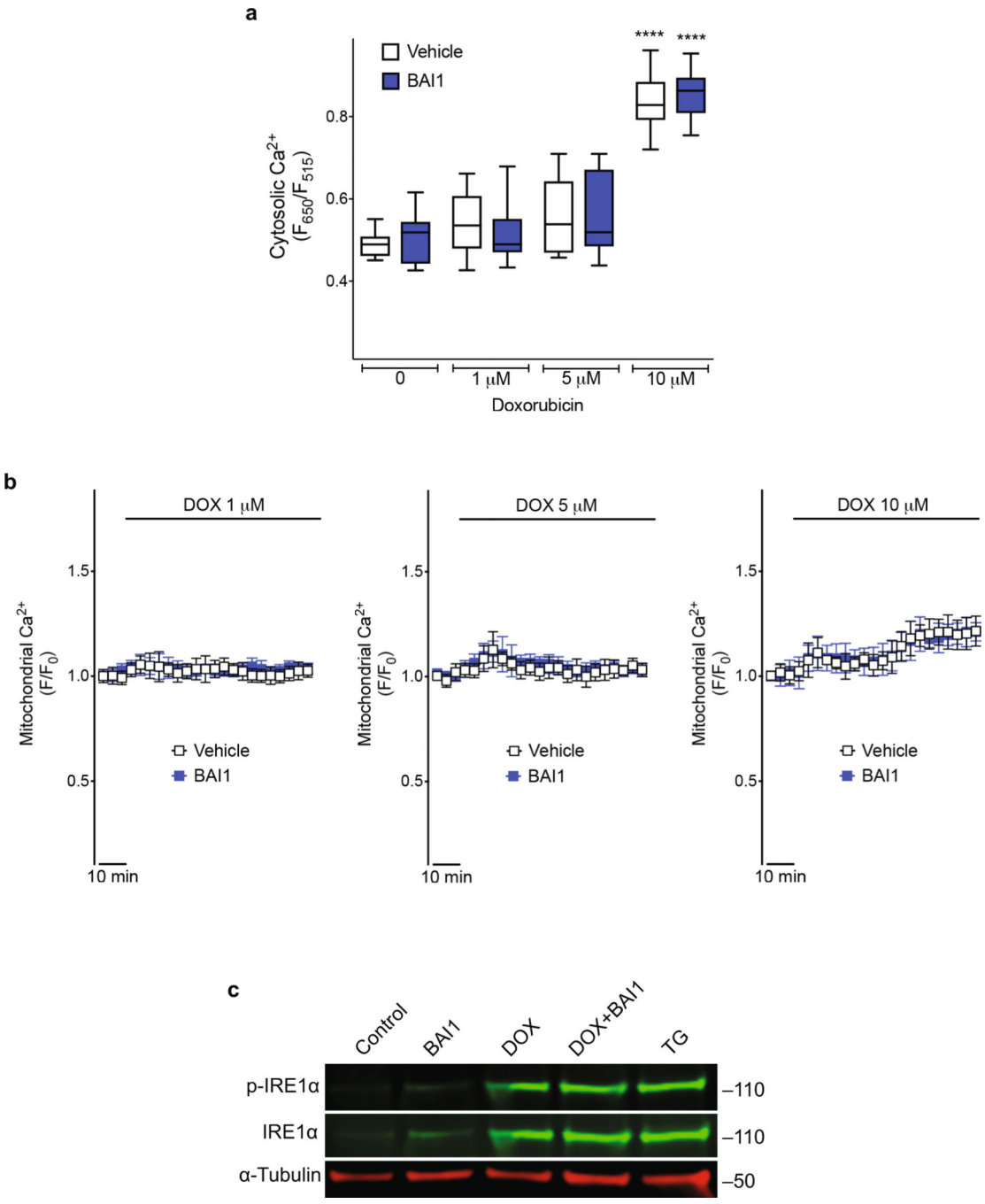

Extended Data Fig. 2 |. BAI1 does not affect baseline or doxorubicin-induced Ca^{2+} handling or IRE1α activation.

a, Cytosolic Ca^{2+} concentrations assessed with Fluo-4 at baseline and following 1 hr treatment with doxorubicin (DOX) in the absence or presence of 1 hr pretreatment with BAI1 1 μM. Box plots depict IQR, horizontal lines show the median, and whiskers represent the minimum and maximum values. n=15, 16 (control); n=18, 19 (DOX 1 μM); n=17, 20 (DOX 5 μM); n=24, 23 (DOX 10 μM) cells. Representative of 2 independent experiments. One-way ANOVA, **** P<0.0001. **b**, Time course of mitochondrial Ca^{2+} concentrations assessed with Rhod-2 at baseline and following 1 hr treatment with DOX in the absence or

presence of pretreatment with BAI1 1 μM. n=28 (DOX 1 μM), n=35 (DOX 5 μM), n=32 (DOX 10 μM) cells. Representative of 2 independent experiments. Data presented as mean ± s.e.m. **c**, Western blot for total and phosphorylated IRE1α in MEFs treated with DOX 10 μM for 12 hr with or without 1 hr pretreatment with BAI1 1 μM. Thapsigargin (TG) 1 μM served as a positive control. Unprocessed images of blots are provided as source data. Representative of 3 independent experiments.

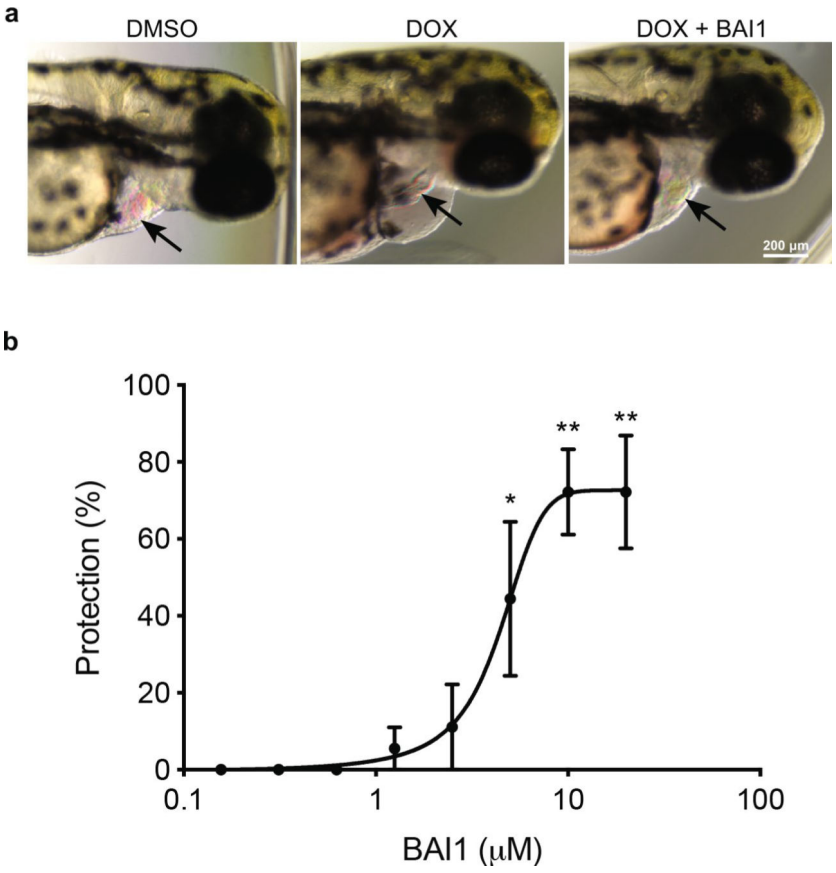

Extended Data Fig. 3 |. BAI1 prevents doxorubicin-induced cardiomyopathy in zebrafish.
a, Zebrafish 30 hr post-fertilization treated with DMSO (control), doxorubicin (DOX), or DOX plus BAI1. Hearts indicated by arrows. Representative images of 3 independent experiments. **b**, BAI1 prevents doxorubicin-induced cardiomyopathy in a dose-dependent manner. Prevention indicates the absence of all 3 of the following manifestations assessed 40 hr post-treatment: decreased cardiac contraction, pericardial edema, and decreased tail blood flow. n=3 independent experiments. One-way ANOVA, * P=0.0456, ** P=0.0011. Data presented as mean ± s.e.m.

a

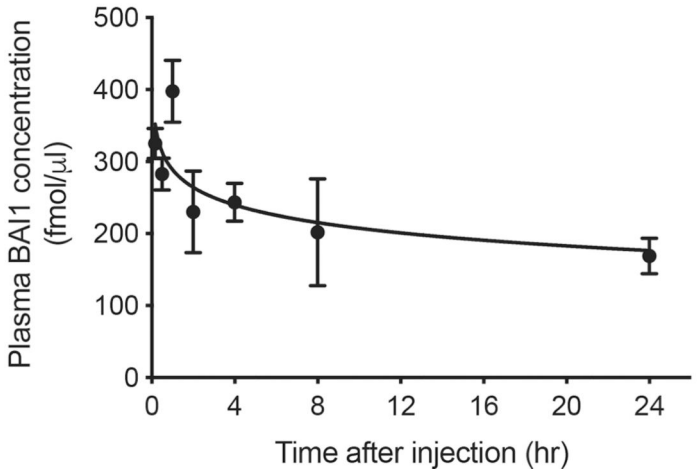

b

Parameter	Estimate	Units
K_{el}	0.015357308	1/hr
$t_{1/2}$	45.13468	hr
C_{max}	397.76	fmol/µL
SE_C_{max}	43.101808	fmol/µL
T_{max}	1	hr
C_0	373.4877	fmol/µL
AUC_{last}	4979.2985	hr · fmol/µL
SE_AUC_{last}	776.55092	hr · fmol/µL
AUC_{inf}	15989.258	hr · fmol/µL
AUC_{extrap}	68.858476	%
V_z	0.004072458	mg/(fmol/µL)/kg
Cl	6.25E-05	mg/(hr · fmol/µL)/kg
$AUMC_{inf}$	1033752.7	hr · hr · fmol/µL
MRT_{inf}	64.65295	hr
V_{ss}	0.004043524	mg/(fmol/µL)/kg

Extended Data Fig. 4 |. Pharmacokinetic analysis of BAI1.

a, Plasma BAI1 concentrations as a function of time following 1 mg/kg intravenous injection into adult male mice. Concentration determined by LC-MS/MS. n=3 males/time point. Data presented as mean ± s.e.m. **b**, Pharmacokinetic parameters estimated by non-compartmental analysis of the plasma BAI1 concentration-time curve. K_{el}: elimination rate constant; $t_{1/2}$: half-life; C_{max}: maximum plasma concentration; SE_C_{max}: standard error of C_{max}; T_{max}: time to reach C_{max}; C_0: concentration at t=0; AUC_{last}: area under the curve from t=0 to the time of the last quantifiable concentration; SE_AUC_{last}: standard error of AUC_{last}; AUC_{inf}: AUC from t=0 to infinity; AUC_{extrap}: extrapolated AUC from last to infinity, expressed as percentage of AUC_{inf}; V_z: volume of distribution following administration; Cl: total body clearance following administration, calculated from dose/AUC; $AUMC_{inf}$: area under the first moment curve from t=0 to infinity; MRT_{inf}: mean residence time, calculated by dividing the $AUMC_{inf}$ by the AUC; V_{ss}: steady-state volume of distribution, calculated from Cl · MRT_{inf}.

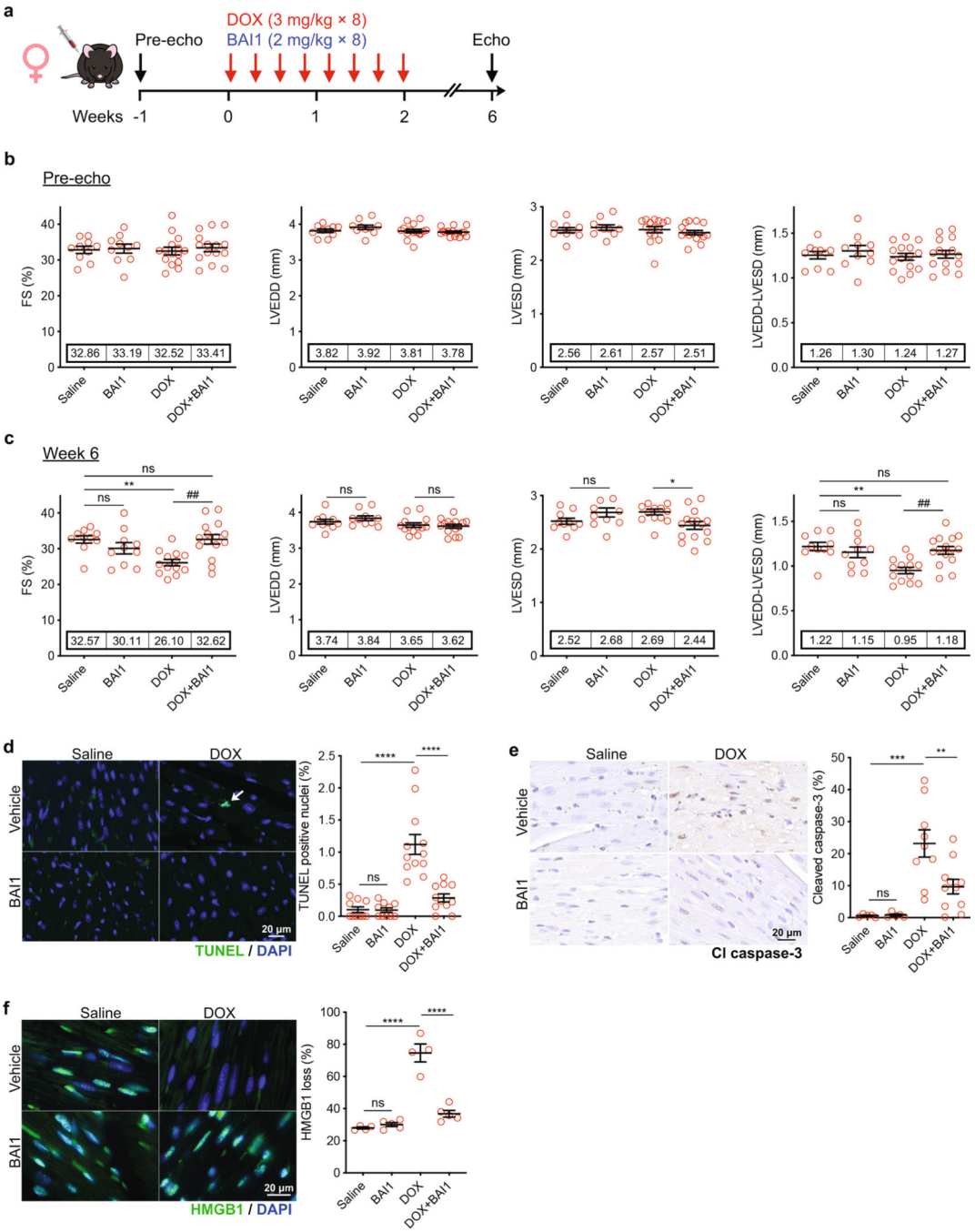

Extended Data Fig. 5 |. BAI1 prevents cardiomyopathy in long-term doxorubicin model (females).

a, Schematic of low-dose, long-term doxorubicin (DOX)-induced cardiomyopathy mouse model. Mice were 12 weeks old at the start of experiment. **b**, Echocardiographic analysis of systolic function including fractional shortening (FS), left ventricular end-diastolic dimension (LVEDD), left ventricular end-systolic dimension (LVESD), and LVEDD-LVESD prior to initiation of treatment. Saline, n=10; BAI1, n=10; DOX, n=15; DOX+BAI1, n=15 females. Mean values are shown on the graphs. **c**, Echocardiographic parameters 4

weeks following the 2-week course of treatment. Saline, n=10; BAI1, n=10; DOX, n=13; DOX+BAI1, n=15 females. Mean values are shown on the graphs. One-way ANOVA, FS: ** P=0.0045, ## P=0.0013; LVESD: * P=0.0368; LVEDD-LVESD: ** P=0.0013, ## P=0.0029. **d**, TUNEL of cardiac sections and quantification to assess apoptosis. Saline, n=10; BAI1, n=10; DOX, n=12; DOX+BAI1, n=11 females. One-way ANOVA, **** P<0.0001. **e**, Cleaved caspase-3 immunohistochemistry of cardiac sections and quantification to assess apoptosis. Saline, n=5; BAI1, n=5; DOX, n=9; DOX+BAI1, n=11 females. One-way ANOVA, ** P=0.0078, *** P=0.0003. **f**, Immunofluorescence for loss of nuclear HMGB1 in cardiac sections and quantification to assess necrosis. Saline, n=4; BAI1, n=5; DOX, n=4; DOX+BAI1, n=5 females. One-way ANOVA, **** P<0.0001. All data presented as mean ± s.e.m. One-way ANOVA, ns P>0.05. The data from the Saline, DOX, and DOX+BAI1 groups for females here are also displayed in Fig. 5b–d along with the corresponding male data in which BAI1 alone was not tested. All four groups are displayed together here so that they can be directly compared within one sex.

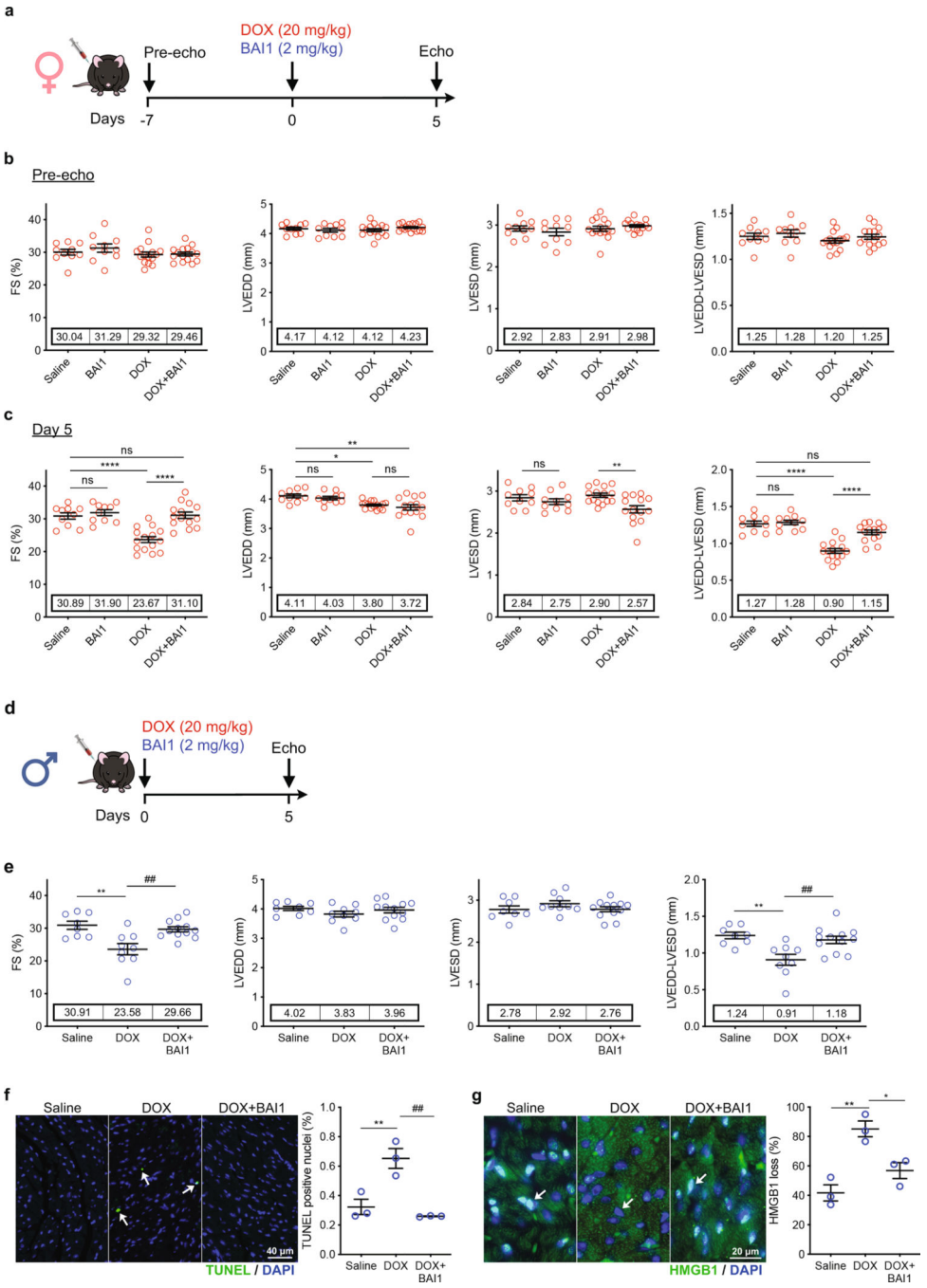

Extended Data Fig. 6 |. BAI1 prevents cardiomyopathy in acute doxorubicin model.

a, Schematic of high-dose, acute doxorubicin (DOX)-induced cardiomyopathy mouse model (females). Mice were 8 weeks old at the start of experiment. **b**, Echocardiographic analysis of systolic function including fractional shortening (FS), left ventricular end-diastolic dimension (LVEDD), left ventricular end-systolic dimension (LVESD), and LVEDD-LVESD prior to initiation of treatment. Saline, n=10; BAI1, n=10; DOX, n=15; DOX+BAI1, n=15 females. Mean values are shown on the graphs. **c**, Echocardiographic parameters 5 days following the single treatment. Saline, n=10; BAI1, n=10; DOX, n=15; DOX+BAI1,

n=14 females. Mean values are shown on the graphs. One-way ANOVA, FS: **** P<0.0001; LVEDD: * P=0.0139, ** P=0.0014; LVESD: ** P=0.0043; LVEDD-LVESD: **** P<0.0001. **d**, Schematic of high-dose, acute DOX-induced cardiomyopathy mouse model (males). Mice were 8 weeks old at the start of experiment. **e**, Echocardiographic parameters 5 days following the single treatment. Saline, n=8; DOX, n=9; DOX+BAI1, n=12 males. Mean values are shown on the graphs. One-way ANOVA, FS: ** P=0.0011, ## P=0.0025; LVEDD-LVESD: ** P=0.0015, ## P=0.0039. **f**, TUNEL of cardiac sections and quantification to assess apoptosis. n=3 males/group. One-way ANOVA, ** P=0.0077, ## P=0.0032. **g**, Immunofluorescence for loss of nuclear HMGB1 in cardiac sections and quantification to assess necrosis. n=3 males/group. One-way ANOVA, * P=0.0235, ** P=0.0031. All data presented as mean ± s.e.m. One-way ANOVA, ns P>0.05.

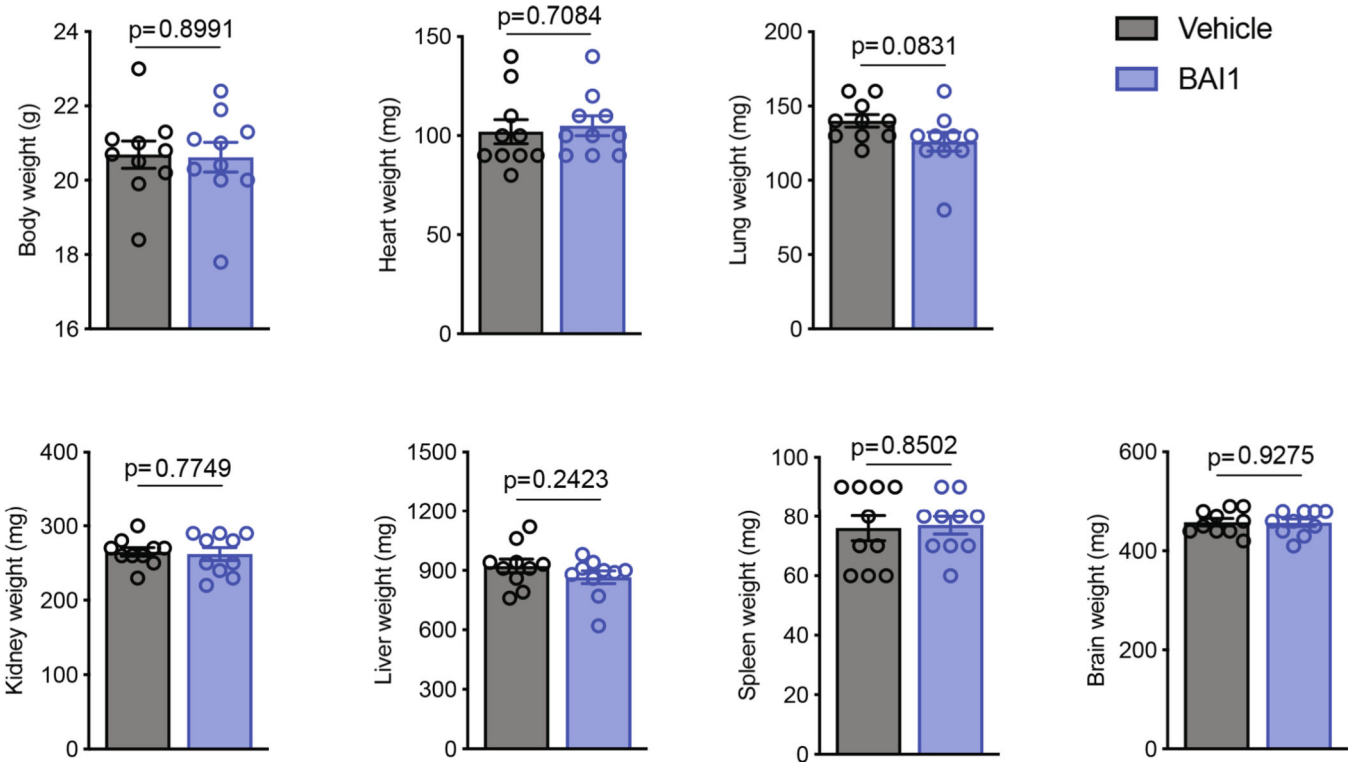

Extended Data Fig. 7 |. BAI1 alone does not affect body or organ weights.

Treatment with BAI1 alone in the long-term model as illustrated in the schematic in Extended Data Fig. 5a. Female mice, 12 weeks old at the start of experiment. n=10 mice/group. All data presented as mean ± s.e.m. P-values from two-tailed Student's *t*-test shown on the graphs.

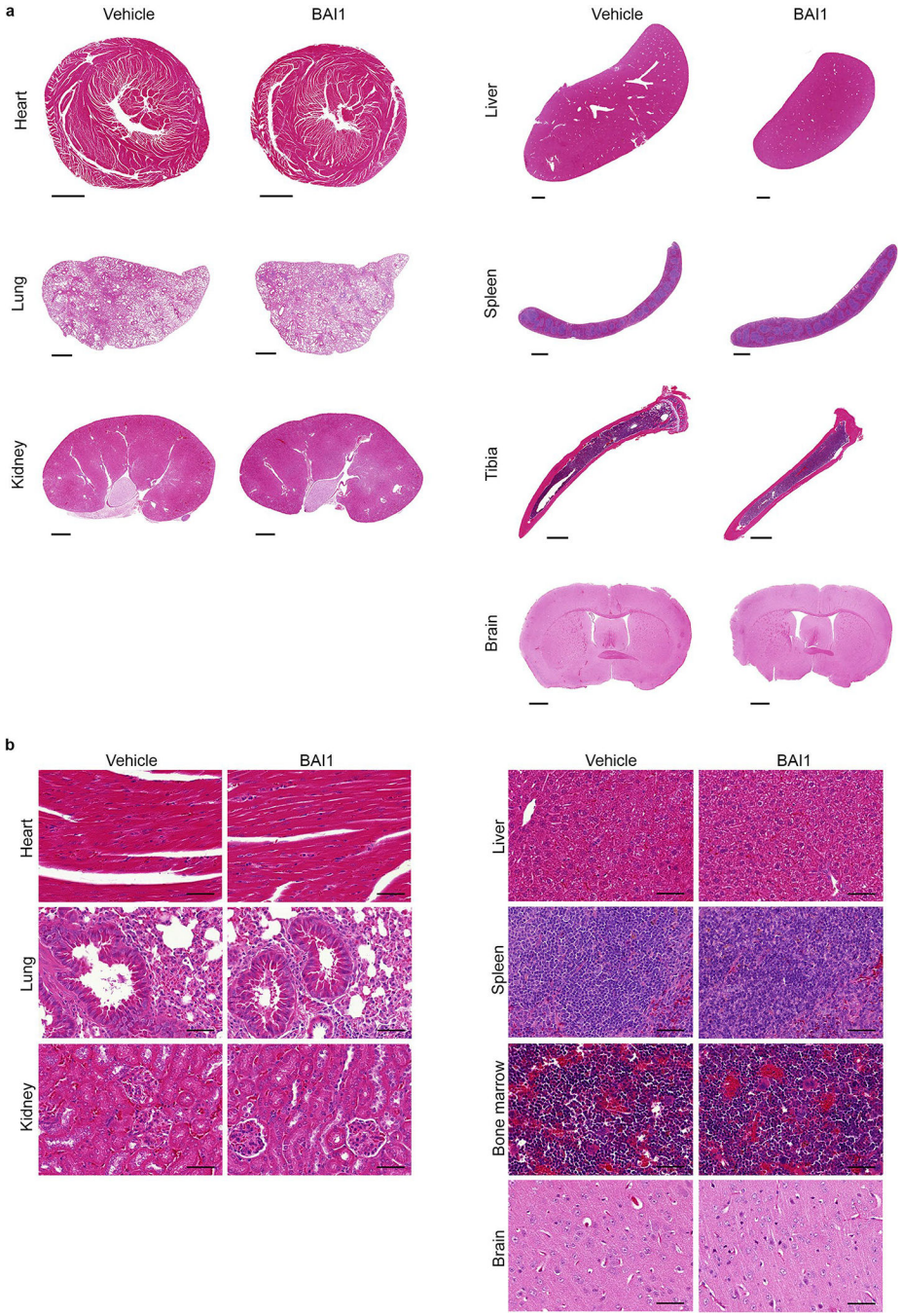

Extended Data Fig. 8 |. BAI1 alone does not affect histology of multiple tissues.

Treatment with BAI1 alone in the long-term model as illustrated in Extended Data Fig. 5a. Female mice, 12 weeks old at the start of experiment. Hematoxylin and eosin staining of mouse tissues. Representative micrographs from n=5 mice/group. Scale bars: a, 1000 μm; b, 50 μm.

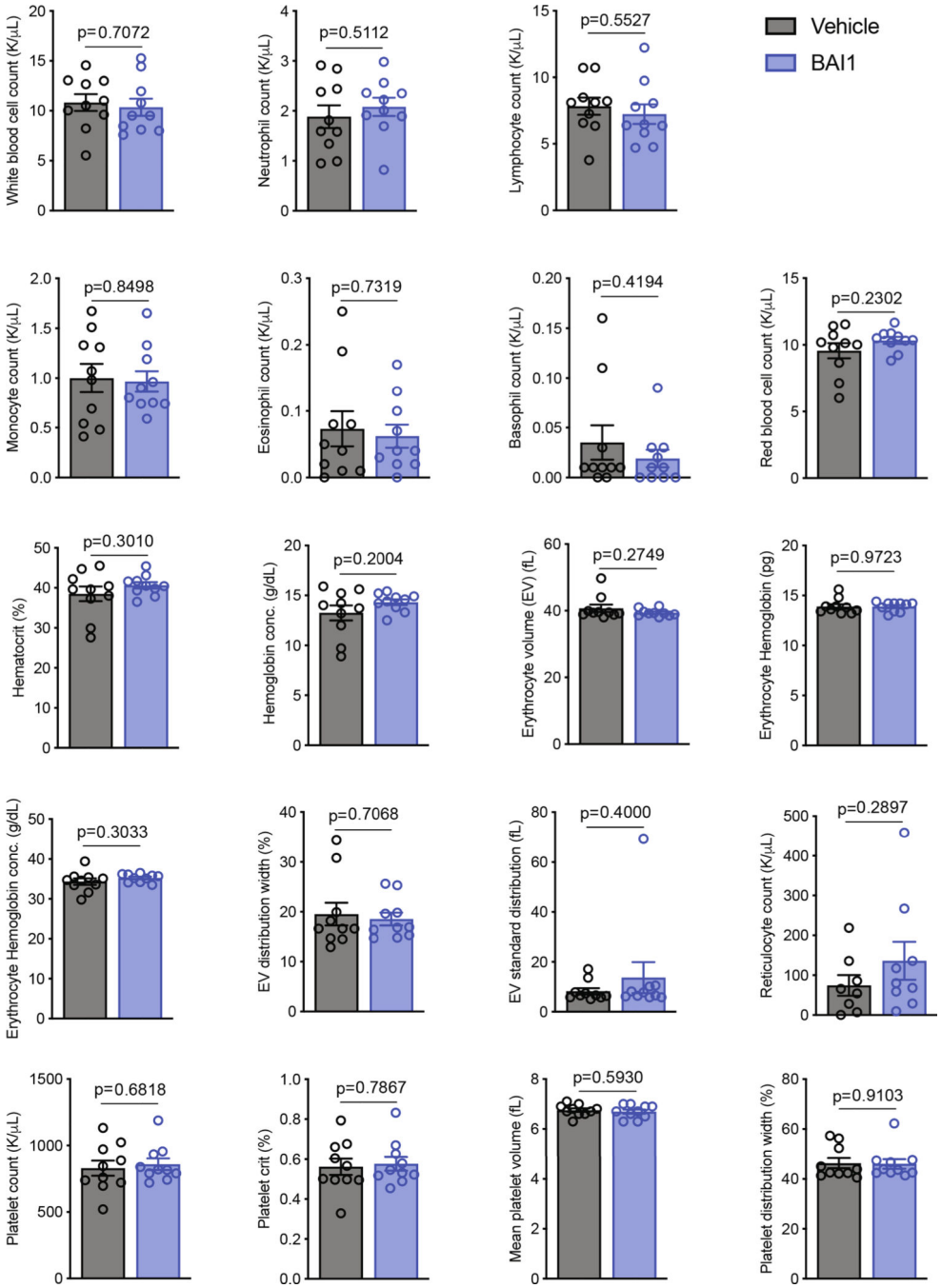

Extended Data Fig. 9 |. BAI1 alone does not affect hematological parameters.

Treatment with BAI1 alone in the long-term model as illustrated in Extended Data Fig. 5a. Female mice, 12 weeks old at the start of experiment. All values are within the normal range for mice. n=10 mice/group. All data presented as mean ± s.e.m. P-values from two-tailed Student's *t*-test shown on the graphs.

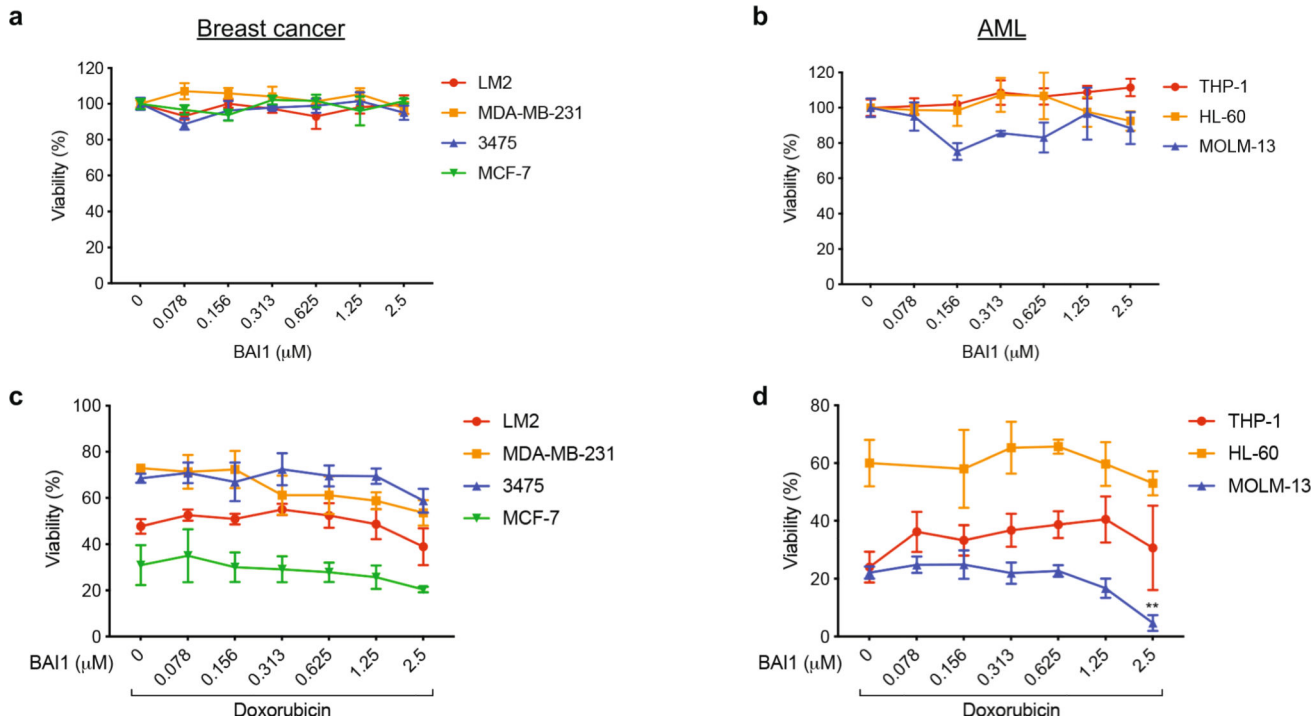

Extended Data Fig. 10 |. BAI1 does not attenuate doxorubicin-induced killing of human cancer cells.

a, **b**, BAI1 alone does not affect cell viability of various cancer cell lines. Cellular viability measured by maintenance of plasma membrane integrity (CytoTox-Glo). **c**, **d**, BAI1 does not interfere with the ability of doxorubicin to kill these cells. For panels c and d, untreated cells (no doxorubicin and no BAI1) assigned a viability of 100% (not shown). All panels, n=3 independent experiments. One-way ANOVA, compared with BAI1 0 μM, ** P=0.0091. All data presented as mean ± s.e.m. For comparison, BAI1 at nanomolar concentrations inhibit cardiomyocyte death (Fig. 4).

Supplementary Material

Refer to Web version on PubMed Central for supplementary material.

Acknowledgements

The authors thank K. B. Margulies and K. Bedi of the University of Pennsylvania for generously providing human heart samples; M. Graham for analysis of pharmacokinetic data; B. Bartholdy for RNA-sequencing analysis; V. Hadad for statistical analysis for in vivo studies; M. Zheng, H. Guzik and A. Vohra for technical assistance with mouse studies, imaging and zebrafish studies. This work was supported by grants from the National Institutes of Health (R01HL128071, R01HL130861, R01HL138475 and R01CA170911 to R.N.K.; R01CA178394 to E.G.; R01HL146691 and R00DK107895 to G.S.; R01CA100324 to J.S.C.; P30CA013330 to the Albert Einstein Cancer Center; T32CA200561 to L.R.S.; 1S10OD019961 Shared Instrumentation Grant to the Einstein Analytical Imaging Facility); American Heart Association (15CSA26240000 and 18SRG34280018 to R.N.K. and E.G.; and 15PRE25080032 Predoctoral Fellowship to D.A.); Harrington Scholar-Innovator Award to R.N.K.; Fondation Leducq (RA15CVD04 to R.N.K. and E.G.); Department of Defense (PR151134P1 to R.N.K); New York State Stem Cell Science (NYSTEM C029154 to the Einstein Stem Cell Isolation and Xenotransplantation Facility); Canadian Institutes for Health Research Foundation Grant to L.A.K.; Breast Cancer Research Foundation to R.B.H.; and John S. LaDue Memorial Fellowship at Harvard Medical School to A.A. R.N.K. was supported by the Dr. Gerald and Myra Dorros Chair in Cardiovascular Disease. Overall support was provided by the Wilf Family Cardiovascular Research Institute.

References

1. Moslehi JJ Cardiovascular toxic effects of targeted cancer therapies. N. Engl. J. Med 375, 1457–1467 (2016). [PubMed: 27732808]
2. Moslehi J, Amgalan D & Kitsis RN Grounding cardio-oncology in basic and clinical science. Circulation 136, 3–5 (2017). [PubMed: 28674089]
3. Middleman E, Luce J & Frei E 3rd Clinical trials with adriamycin. Cancer 28, 844–850 (1971). [PubMed: 5111740]
4. Lefrak EA, Pitha J, Rosenheim S & Gottlieb JA A clinicopathologic analysis of adriamycin cardiotoxicity. Cancer 32, 302–314 (1973). [PubMed: 4353012]
5. Tewey KM, Rowe TC, Yang L, Halligan BD & Liu LF Adriamycin-induced DNA damage mediated by mammalian DNA topoisomerase II. Science 226, 466–468 (1984). [PubMed: 6093249]
6. Zhang S et al. Identification of the molecular basis of doxorubicin-induced cardiotoxicity. Nat. Med 18, 1639–1642 (2012). [PubMed: 23104132]
7. Ichikawa Y et al. Cardiotoxicity of doxorubicin is mediated through mitochondrial iron accumulation. J. Clin. Invest 124, 617–630 (2014). [PubMed: 24382354]
8. Zhou S, Starkov A, Froberg MK, Leino RL & Wallace KB Cumulative and irreversible cardiac mitochondrial dysfunction induced by doxorubicin. Cancer Res. 61, 771–777 (2001). [PubMed: 11212281]
9. Lim CC et al. Anthracyclines induce calpain-dependent titin proteolysis and necrosis in cardiomyocytes. J. Biol. Chem 279, 8290–8299 (2004). [PubMed: 14676206]
10. Li DL et al. Doxorubicin blocks cardiomyocyte autophagic flux by inhibiting lysosome acidification. Circulation 133, 1668–1687 (2016). [PubMed: 26984939]
11. Renu K, V GA, P BT & Arunachalam S Molecular mechanism of doxorubicin-induced cardiomyopathy - An update. Eur. J. Pharmacol 818, 241–253 (2018). [PubMed: 29074412]
12. Zhang YW, Shi J, Li YJ & Wei L Cardiomyocyte death in doxorubicin-induced cardiotoxicity. Arch. Immunol. Ther. Exp. (Warsz) 57, 435–445 (2009). [PubMed: 19866340]
13. Walensky LD & Gavathiotis E BAX unleashed: the biochemical transformation of an inactive cytosolic monomer into a toxic mitochondrial pore. Trends Biochem. Sci 36, 642–652 (2011). [PubMed: 21978892]
14. Whelan RS, Kaplinskiy V & Kitsis RN Cell death in the pathogenesis of heart disease: mechanisms and significance. Annu. Rev. Physiol 72, 19–44 (2010). [PubMed: 20148665]
15. Whelan RS et al. BAX regulates primary necrosis through mitochondrial dynamics. Proc. Natl Acad. Sci. USA 109, 6566–6571 (2012). [PubMed: 22493254]
16. Karch J et al. BAX and BAK function as the outer membrane component of the mitochondrial permeability pore in regulating necrotic cell death in mice. eLife 2, e00772 (2013). [PubMed: 23991283]
17. Gavathiotis E et al. BAX activation is initiated at a novel interaction site. Nature 455, 1076–1081 (2008). [PubMed: 18948948]
18. Gavathiotis E, Reyna DE, Davis ML, Bird GH & Walensky LD BH3-triggered structural reorganization drives the activation of proapoptotic BAX. Mol. Cell 40, 481–492 (2010). [PubMed: 21070973]
19. Ferreira de Souza T et al. Anthracycline therapy is associated with cardiomyocyte atrophy and preclinical manifestations of heart disease. JACC Cardiovasc. Imaging 11, 1045–1055 (2018). [PubMed: 30092965]
20. Neilan TG et al. Left ventricular mass in patients with a cardiomyopathy after treatment with anthracyclines. Am. J. Cardiol 110, 1679–1686 (2012). [PubMed: 22917553]
21. Jordan JH et al. Left ventricular mass change after anthracycline chemotherapy. Circ. Heart Fail 11, e004560 (2018). [PubMed: 29991488]
22. Zhu W et al. Acute doxorubicin cardiotoxicity is associated with p53-induced inhibition of the mammalian target of rapamycin pathway. Circulation 119, 99–106 (2009). [PubMed: 19103993]
23. Scaffidi P, Misteli T & Bianchi ME Release of chromatin protein HMGB1 by necrotic cells triggers inflammation. Nature 418, 191–195 (2002). [PubMed: 12110890]

24. Bombrun A et al. 3,6-dibromocarbazole piperazine derivatives of 2-propanol as first inhibitors of cytochrome c release via BAX channel modulation. J. Med. Chem 46, 4365–4368 (2003). [PubMed: 14521400]
25. Peixoto PM, Ryu SY, Bombrun A, Antonsson B & Kinnally KW MAC inhibitors suppress mitochondrial apoptosis. Biochem. J 423, 381–387 (2009). [PubMed: 19691447]
26. Garner TP et al. Small-molecule allosteric inhibitors of BAX. Nat. Chem. Biol 15, 322–330 (2019). [PubMed: 30718816]
27. Hsu YT & Youle RJ Nonionic detergents induce dimerization among members of the Bcl-2 family. J. Biol. Chem 272, 13829–13834 (1997). [PubMed: 9153240]
28. Antonsson B, Montessuit S, Sanchez B & Martinou JC BAX is present as a high molecular weight oligomer/complex in the mitochondrial membrane of apoptotic cells. J. Biol. Chem 276, 11615–11623 (2001). [PubMed: 11136736]
29. Scorrano L et al. BAX and BAK regulation of endoplasmic reticulum Ca^{2+}: a control point for apoptosis. Science 300, 135–139 (2003). [PubMed: 12624178]
30. Oakes SA et al. Proapoptotic BAX and BAK regulate the type 1 inositol trisphosphate receptor and calcium leak from the endoplasmic reticulum. Proc. Natl Acad. Sci. USA 102, 105–110 (2005). [PubMed: 15613488]
31. Hetz C et al. Proapoptotic BAX and BAK modulate the unfolded protein response by a direct interaction with IRE1α. Science 312, 572–576 (2006). [PubMed: 16645094]
32. Liu Y et al. Visnagin protects against doxorubicin-induced cardiomyopathy through modulation of mitochondrial malate dehydrogenase. Sci. Transl. Med 6, 266ra170 (2014).
33. Minn AJ et al. Genes that mediate breast cancer metastasis to lung. Nature 436, 518–524 (2005). [PubMed: 16049480]
34. Patsialou A et al. Selective gene-expression profiling of migratory tumor cells in vivo predicts clinical outcome in breast cancer patients. Breast Cancer Res. 14, R139 (2012). [PubMed: 23113900]
35. Karagiannis GS et al. Neoadjuvant chemotherapy induces breast cancer metastasis through a TMEM-mediated mechanism. Sci. Transl. Med 9, eaan0026 (2017). [PubMed: 28679654]
36. Krivtsov AV et al. Transformation from committed progenitor to leukaemia stem cell initiated by MLL-AF9. Nature 442, 818–822 (2006). [PubMed: 16862118]
37. Somervaille TC & Cleary ML Identification and characterization of leukemia stem cells in murine MLL-AF9 acute myeloid leukemia. Cancer Cell 10, 257–268 (2006). [PubMed: 17045204]
38. Letai AG Diagnosing and exploiting cancer's addiction to blocks in apoptosis. Nat. Rev. Cancer 8, 121–132 (2008). [PubMed: 18202696]
39. Montero J et al. Drug-induced death signaling strategy rapidly predicts cancer response to chemotherapy. Cell 160, 977–989 (2015). [PubMed: 25723171]
40. Sarosiek KA et al. Developmental regulation of mitochondrial apoptosis by c-Myc governs age- and tissue-specific sensitivity to cancer therapeutics. Cancer Cell 31, 142–156 (2017). [PubMed: 28017613]
41. Polster BM, Basanez G, Young M, Suzuki M & Fiskum G Inhibition of BAX-induced cytochrome c release from neural cell and brain mitochondria by dibucaine and propranolol. J. Neurosci 23, 2735–2743 (2003). [PubMed: 12684459]
42. Hetz C et al. BAX channel inhibitors prevent mitochondrion-mediated apoptosis and protect neurons in a model of global brain ischemia. J. Biol. Chem 280, 42960–42970 (2005). [PubMed: 16219766]
43. Niu X et al. A small-molecule inhibitor of BAX and BAK oligomerization prevents genotoxic cell death and promotes neuroprotection. Cell Chem. Biol 24, 493–506 (2017). [PubMed: 28392146]
44. Ky B, Vejpongsa P, Yeh ET, Force T & Moslehi JJ Emerging paradigms in cardiomyopathies associated with cancer therapies. Circ. Res 113, 754–764 (2013). [PubMed: 23989717]
45. Garcia-Pavia P et al. Genetic variants associated with cancer therapy-induced cardiomyopathy. Circulation 140, 31–41 (2019). [PubMed: 30987448]

46. Rambal AA, Panaguiton ZL, Kramer L, Grant S & Harada H MEK inhibitors potentiate dexamethasone lethality in acute lymphoblastic leukemia cells through the pro-apoptotic molecule BIM. Leukemia 23, 1744–1754 (2009). [PubMed: 19404317]
47. Meng J et al. Apoptosis induction by MEK inhibition in human lung cancer cells is mediated by BIM. PLoS ONE 5, e13026 (2010). [PubMed: 20885957]
48. Kirshenbaum LA & Schneider MD Adenovirus E1A represses cardiac gene transcription and reactivates DNA synthesis in ventricular myocytes, via alternative pocket protein- and p300-binding domains. J. Biol. Chem 270, 7791–7794 (1995). [PubMed: 7713869]
49. Kirshenbaum LA, MacLellan WR, Mazur W, French BA & Schneider MD Highly efficient gene transfer into adult ventricular myocytes by recombinant adenovirus. J. Clin. Invest 92, 381–387 (1993). [PubMed: 8326005]
50. Uchime O et al. Synthetic antibodies inhibit Bcl-2-associated X protein (BAX) through blockade of the N-terminal activation site. J. Biol. Chem. 291, 89–102 (2016). [PubMed: 26565029]
51. Gavathiotis E, Reyna DE, Bellairs JA, Leshchiner ES & Walensky LD Direct and selective small-molecule activation of proapoptotic BAX. Nat. Chem. Biol 8, 639–645 (2012). [PubMed: 22634637]
52. Youle RJ & Strasser A The BCL-2 protein family: opposing activities that mediate cell death. Nat. Rev. Mol. Cell Biol 9, 47–59 (2008). [PubMed: 18097445]
53. Regula KM, Ens K & Kirshenbaum LA Inducible expression of BNIP3 provokes mitochondrial defects and hypoxia-mediated cell death of ventricular myocytes. Circ. Res 91, 226–231 (2002). [PubMed: 12169648]
54. Santulli G, Xie W, Reiken SR & Marks AR Mitochondrial calcium overload is a key determinant in heart failure. Proc. Natl Acad. Sci. USA 112, 11389–11394 (2015). [PubMed: 26217001]
55. Lombardi A, Trimarco B, Iaccarino G & Santulli G Impaired mitochondrial calcium uptake caused by tacrolimus underlies β-cell failure. Cell Commun. Signal 15, 47 (2017). [PubMed: 29132395]
56. Rohrbach P et al. Quantitative calcium measurements in subcellular compartments of *Plasmodium falciparum*-infected erythrocytes. J. Biol. Chem 280, 27960–27969 (2005). [PubMed: 15927958]
57. Walczysko P, Wagner E & Albrechtova JT Use of co-loaded Fluo-3 and Fura Red fluorescent indicators for studying the cytosolic Ca^{2+} concentrations distribution in living plant tissue. Cell Calcium 28, 23–32 (2000). [PubMed: 10942701]
58. Waning DL et al. Excess TGF-β mediates muscle weakness associated with bone metastases in mice. Nat. Med. 21, 1262–1271 (2015). [PubMed: 26457758]
59. Stypmann J et al. Echocardiographic assessment of global left ventricular function in mice. Lab Animal 43, 127–137 (2009).
60. Gao S, Ho D, Vatner DE & Vatner SF Echocardiography in mice. Curr. Protoc. Mouse Biol 1, 71–83 (2011). [PubMed: 21743841]
61. Medina-Ramirez CM et al. Apoptosis inhibitor ARC promotes breast tumorigenesis, metastasis, and chemoresistance. Cancer Res. 71, 7705–7715 (2011). [PubMed: 22037876]
62. Chen W et al. Malignant transformation initiated by Mll-AF9: gene dosage and critical target cells. Cancer Cell 13, 432–440 (2008). [PubMed: 18455126]
63. Ryan J, Montero J, Rocco J & Letai A iBH3: simple, fixable BH3 profiling to determine apoptotic priming in primary tissue by flow cytometry. Biol. Chem 397, 671–678 (2016). [PubMed: 26910743]
64. Ryan J & Letai A BH3 profiling in whole cells by fluorimeter or FACS. Methods 61, 156–164 (2013). [PubMed: 23607990]

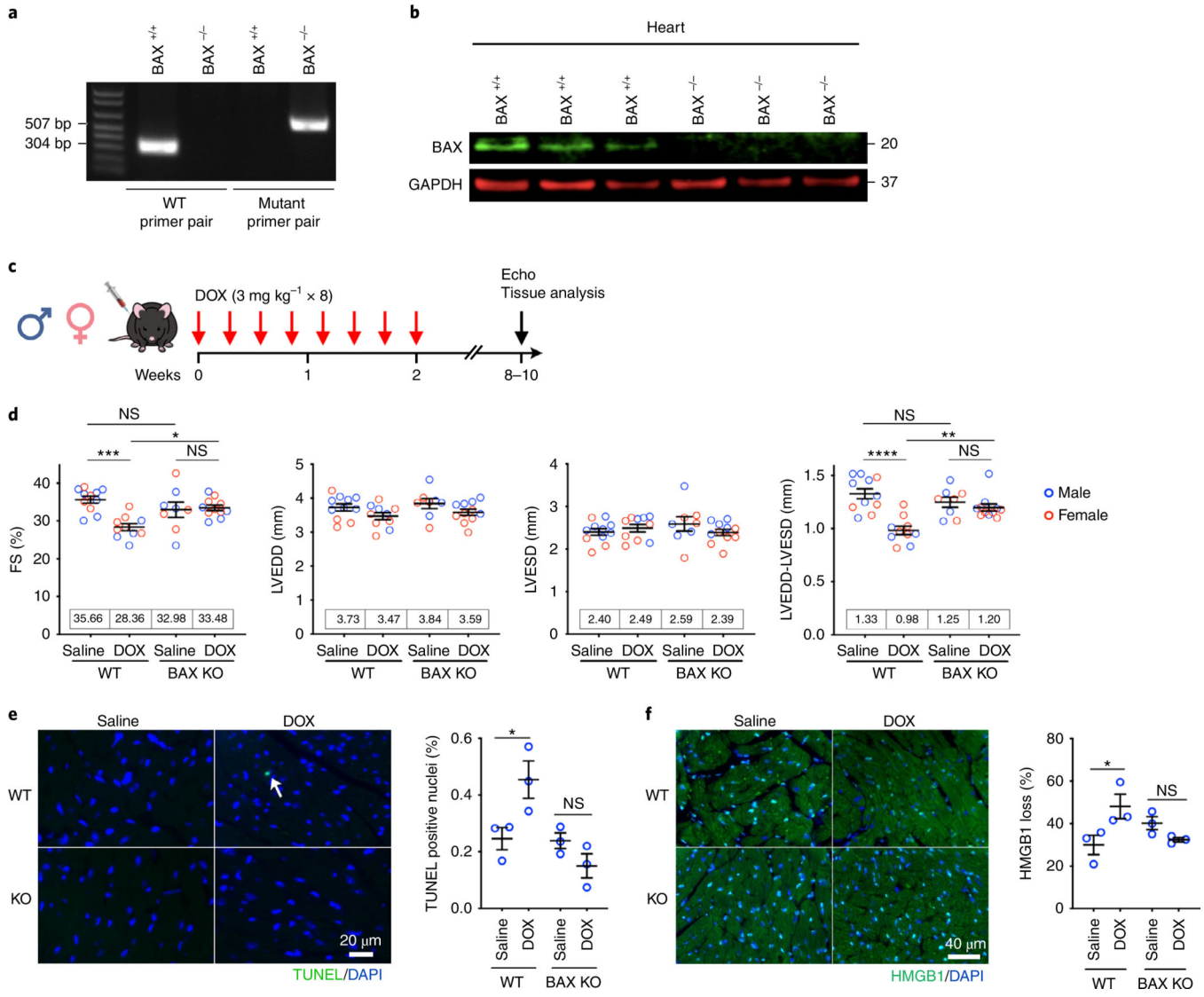

Fig. 1 |. Deletion of BAX protects against doxorubicin-induced cardiomyopathy.

a, BAX genotyping of WT and germline BAX KO mice with primer pairs specific for WT and deleted BAX alleles. **b**, Western blot for BAX in mice hearts. Unprocessed images of blots are provided as source data. **a**,**b** are representative of three independent experiments. **c**, Schematic of a low-dose, long-term doxorubicin (DOX)-induced cardiomyopathy mouse model. **d**, Echocardiographic analysis of systolic function, including FS, LVEDD, LVESD and LVEDD-LVESD. These data represent two independent experiments, one consisting of males (12–15 weeks of age at the start of experiment; blue circles) and the other, females (8–10 weeks of age at the start of experiment; red circles). WT-saline, $n = 7$ males, 4 females; WT-DOX, $n = 4$ males, 6 females; KO-saline, $n = 4$ males, 4 females; KO-DOX, $n = 5$ males, 6 females. Mean values are shown on the graphs. One-way analysis of variance (ANOVA), FS: $^{*}P = 0.0120$, $^{***}P = 0.0002$; LVEDD-LVESD: $^{**}P = 0.0040$, $^{****}P < 0.0001$. **e**, TUNEL of cardiac sections and quantification to assess apoptosis ($n = 3$ males per group). One-way ANOVA, $^{*}P = 0.0246$. **f**, Immunofluorescence for loss of nuclear HMGB1

in cardiac sections and quantification to assess necrosis. Aqua color indicates presence of HMGB1 (HMGB1 + 4,6-diamidino-2-phenylindole (DAPI)) and blue color indicates loss of HMGB1 (DAPI alone) (n = 3 males per group). One-way ANOVA, *P = 0.0249. All data are presented as mean ± s.e.m. One-way ANOVA, NS, not significant $P > 0.05$.

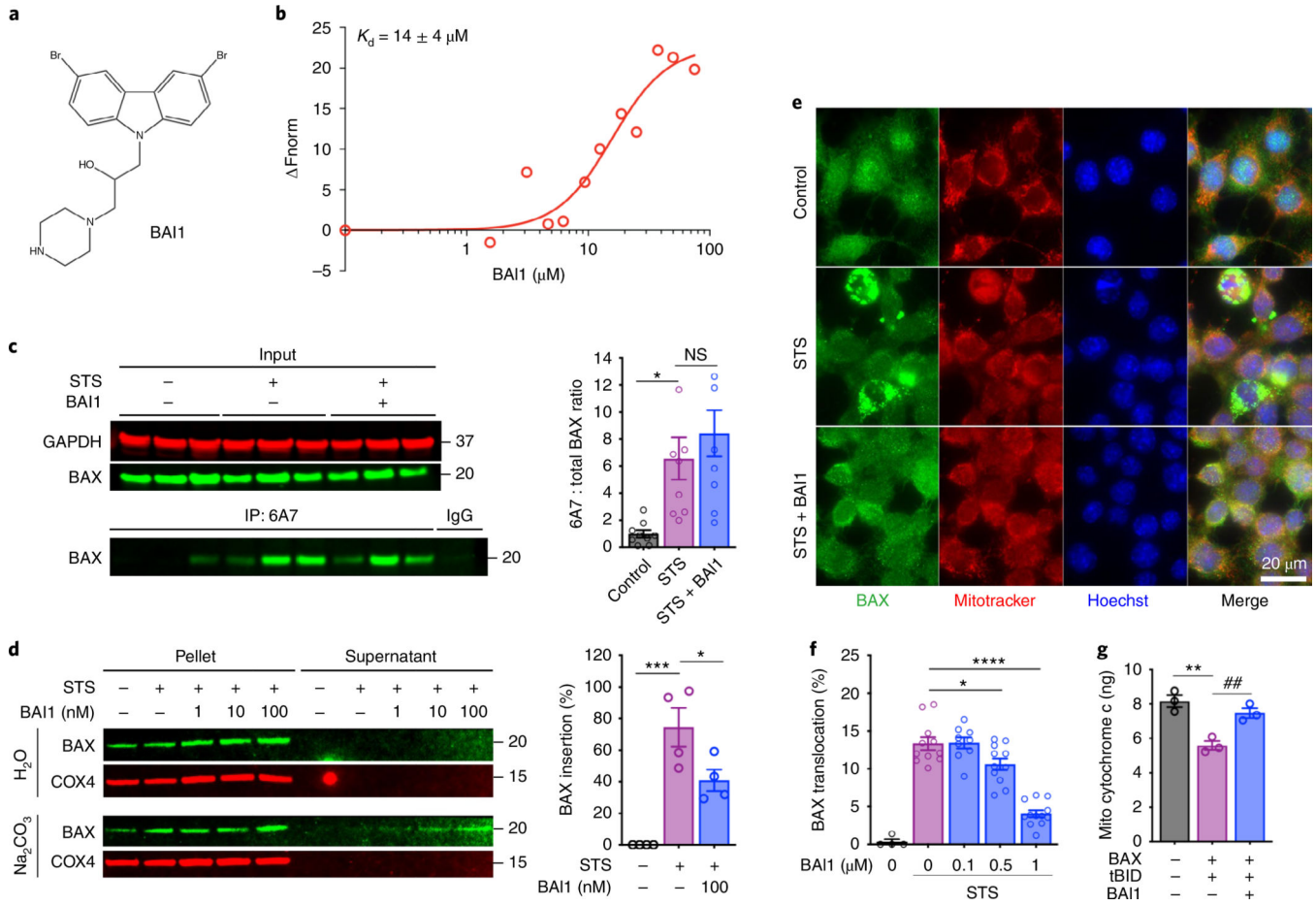

Fig. 2 |. BAI1 binds BAX directly to inhibit its mitochondrial insertion and translocation.

a, Chemical structure of BAI1. **b**, Microscale thermophoretic analysis of BAI1 binding BAX. ΔFnorm, normalized change in fluorescence. Representative of three independent experiments. **c**, Lack of an effect of BAI1 (0.1 μM) on early conformational changes in BAX activation in staurosporine (STS)-treated MEFs as assessed by exposure of 6A7 epitope. Three independent experiments each with three independent immunoprecipitations per group. One-way ANOVA, $*P = 0.0141$, NS, $P > 0.05$. **d**, BAI1 inhibits BAX insertion into the OMM. Only noninserted BAX can be recovered from isolated mitochondria by treatment with strong alkali ($n = 4$ independent experiments). One-way ANOVA, $*P = 0.0301$, $***P = 0.0002$. **e**,**f**, Inhibition of BAX mitochondrial translocation by BAI1. **e**, Representative images of immunofluorescence for BAX translocation in WT MEFs. **f**, Quantification of percentage of cells with BAX puncta ($n = 4$, 11, 9, 11 and 12 images). Data are representative of five independent experiments. One-way ANOVA, $*P = 0.0237$, $****P < 0.0001$. **g**, BAI1 (10 μM) inhibits BAX-dependent cytochrome *c* release as assessed by ELISA. Mitochondria isolated from BAX/BAK DKO MEFs were incubated with recombinant BAX and tBID ($n = 3$ independent mitochondrial isolates per group). Representative of three independent experiments. One-way ANOVA, $**P = 0.0016$, $^{\#\#}P = 0.0074$. Data in **c**,**d**,**f**,**g** are presented as mean ± s.e.m. Unprocessed images of blots are provided as source data.

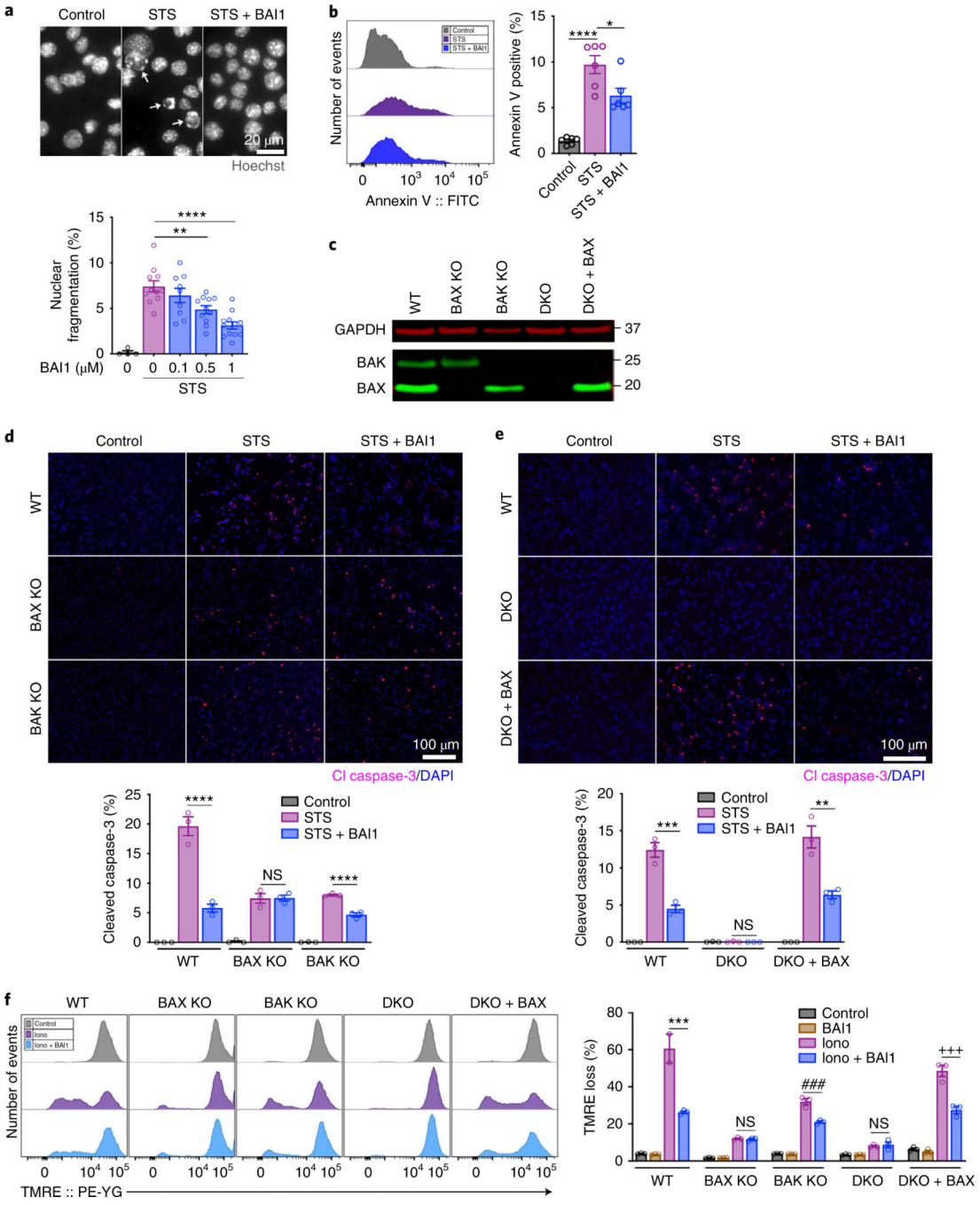

Fig. 3 |. BAI1 inhibits BAX-dependent apoptosis and necrosis.

a, BAI1 inhibits nuclear fragmentation of STS-treated WT MEFs as assessed by Hoechst staining (n = 4, 11, 9, 11 and 12 images). Data are representative of three independent experiments. One-way ANOVA, $^{**}P = 0.005$, $^{****}P < 0.0001$. **b**, BAI1 (0.25 μM) inhibits annexin V binding to externalized phosphatidylserine in STS-treated WT MEFs as assessed by flow-cytometric analysis. Three independent experiments each with two independent wells per group. One-way ANOVA, $^{*}P = 0.0146$, $^{****}P < 0.0001$. **c**, Western blot for BAX and BAK in MEFs of the indicated genotypes. Unprocessed images of blots are provided as

source data. Representative of three independent experiments. **d**, BAX is necessary for inhibition of apoptosis by BAI1. Immunofluorescence analysis of cleaved caspase-3 in WT, BAX KO and BAK KO MEFs treated with STS ($n = 3$ independent experiments). One-way ANOVA, $^{****}P < 0.0001$. **e**, BAX is sufficient for inhibition of apoptosis by BAI1. Immunofluorescence analysis of cleaved caspase-3 in STS-treated MEFs: WT, DKO and DKO reconstituted stably with physiological levels of BAX (DKO + BAX) ($n = 3$ independent experiments). One-way ANOVA, $^{**}P = 0.0022$, $^{***}P = 0.0003$. **f**, BAX is necessary and sufficient for inhibition of necrosis by BAI1. Flow cytometric analysis of mitochondrial depolarization (tetramethylrhodamine ethyl ester (TMRE) loss) in ionomycin (Iono)-treated MEFs of the indicated genotypes ($n = 3$ independent wells per group). Data are representative of four independent experiments. One-way ANOVA, $^{***}P = 0.0002$, $^{\#\#\#}P = 0.0001$, $^{+++}P = 0.0002$. BAI1 concentration was 1 μM in **d**–**f**. All data are presented as mean ± s.e.m. One-way ANOVA, NS, $P > 0.05$.

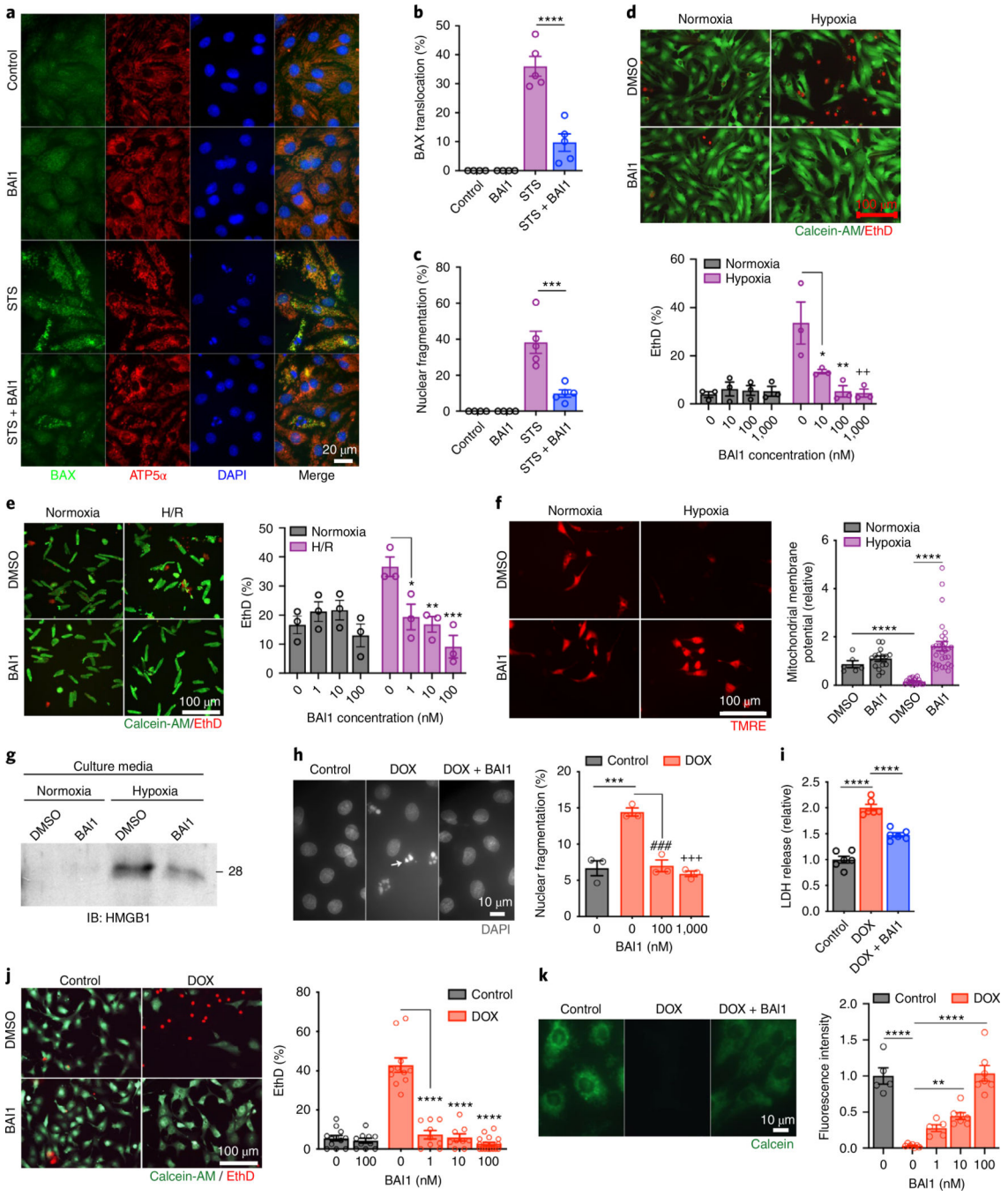

Fig. 4 |. BAI1 inhibits apoptosis and necrosis in primary cardiomyocytes.

a–**c**, BAI1 (1 μM) inhibits STS-induced BAX translocation to mitochondria and apoptosis. Data are representative of three independent experiments. Representative images of neonatal rat cardiomyocytes treated as indicated and immunostained for BAX, ATP5α (mitochondrial protein) and DAPI (**a**). Quantification of BAX mitochondrial translocation ($n = 4, 4, 5$ and 5 images) (**b**). Quantification of nuclear fragmentation ($n = 4, 4, 5$ and 5 images) (**c**). One-way ANOVA, ***$P = 0.0003$. **d**–**g**, BAI1 inhibits hypoxia- or hypoxia/reoxygenation (H/R)-induced loss of plasma membrane integrity and mitochondrial depolarization. Entry of

ethidium homodimer (EthD) into neonatal rat cardiomyocytes ($n = 3$ independent experiments). Calcein-AM, calcein-acetoxymethyl ester (**d**). One-way ANOVA, $*P = 0.0367$, $**P = 0.0065$, $^{++}P = 0.0055$. Entry of EthD into adult rat cardiomyocytes ($n = 3$ images per group) (**e**). Representative of two independent experiments. One-way ANOVA, $*P = 0.0194$, $**P = 0.0085$, $***P = 0.0009$. Mitochondrial membrane potential (TMRE) in neonatal rat cardiomyocytes (**f**). BAI1 concentration 1 μM. $n = 20, 29, 34, 43$ cells of one independent experiment. Western blot of medium for HMGB1 release from neonatal rat cardiomyocytes (**g**). BAI1 concentration 1 μM. Equal volumes of serum-free media were loaded. Unprocessed image of the blot is provided as source data. Data are representative of two independent experiments. **h**, BAI1 inhibits DOX-induced apoptosis in neonatal rat cardiomyocytes as assessed by nuclear fragmentation ($n = 3$ independent experiments). One-way ANOVA, $***P = 0.0002$, $^{###}P = 0.0003$, $^{+++}P = 0.0001$. **i**–**k**, BAI1 inhibits DOX-induced necrosis in neonatal rat cardiomyocytes. Loss of plasma membrane integrity as assessed by release of lactate dehydrogenase (LDH) (**i**). BAI1 concentration 1 μM ($n = 6$ independent wells per group). Data are representative of two independent experiments. Entry of EthD ($n = 12, 10, 11, 9, 9$ and 17 images) (**j**). Data are representative of two independent experiments. Mitochondrial calcein retention ($n = 5, 7, 5, 7$ and 7 images) (**k**). Data are representative of two independent experiments. One-way ANOVA, $**P = 0.0012$. All data are presented as mean ± s.e.m. One-way ANOVA, $****P < 0.0001$.

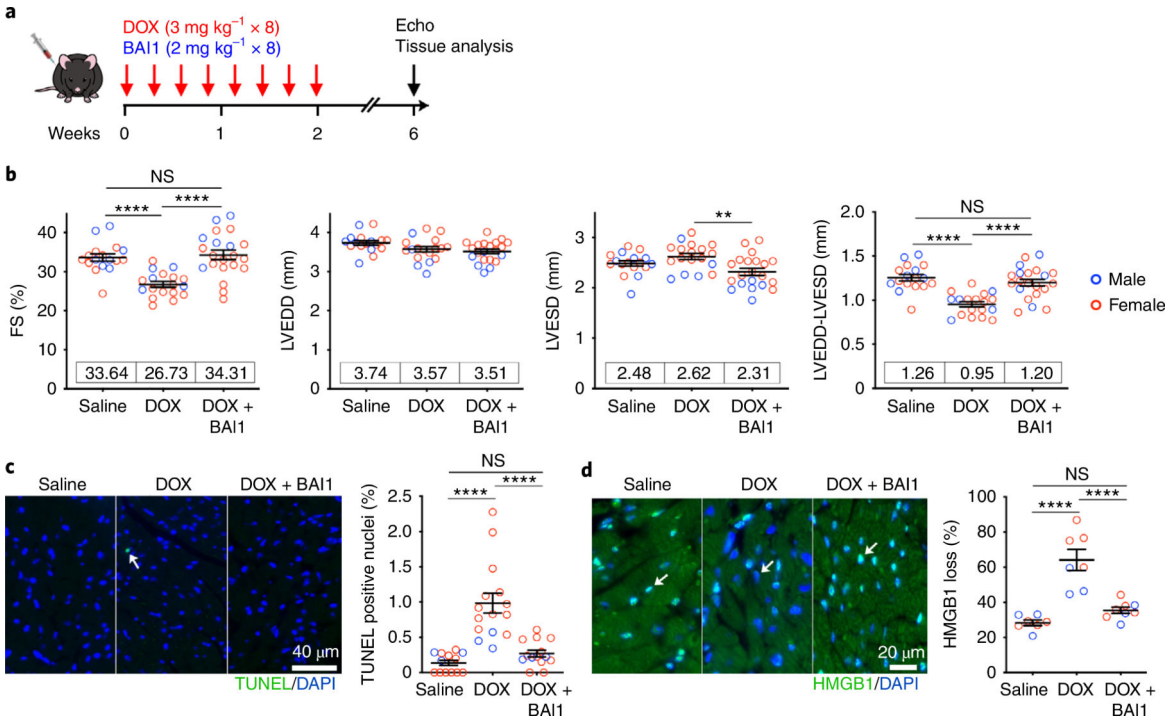

Fig. 5 |. BAI1 prevents doxorubicin-induced cardiomyopathy.

a, Schematic of a low-dose, long-term DOX-induced cardiomyopathy mouse model for testing BAI1. **b**, Echocardiographic analysis of systolic function including FS, LVEDD, LVESD and LVEDD-LVESD. These data represent two independent experiments, one consisting of males (blue circles) and the other females (red circles) with mice of both sexes 12–15 weeks old at the start of experiment. Saline, $n = 7$ males, 10 females; DOX, $n = 5$ males, 13 females; DOX + BAI1, $n = 6$ males, 15 females. Mean values are shown on the graphs. One-way ANOVA, $^{**}P = 0.0023$. **c**, TUNEL of cardiac sections and quantification to assess apoptosis. Saline, $n = 3$ males, 10 females; DOX, $n = 3$ males, 12 females; DOX + BAI1, $n = 3$ males, 11 females. **d**, Immunofluorescence for loss of nuclear HMGB1 in cardiac sections and quantification to assess necrosis. Saline, $n = 3$ males, 4 females; DOX, $n = 3$ males, 4 females; DOX + BAI1, $n = 3$ males, 5 females. All data are presented as mean ± s.e.m. One-way ANOVA, $^{****}P < 0.0001$, NS, $P > 0.05$. Effects of BAI1 alone in this model shown in Extended Data Fig. 5.

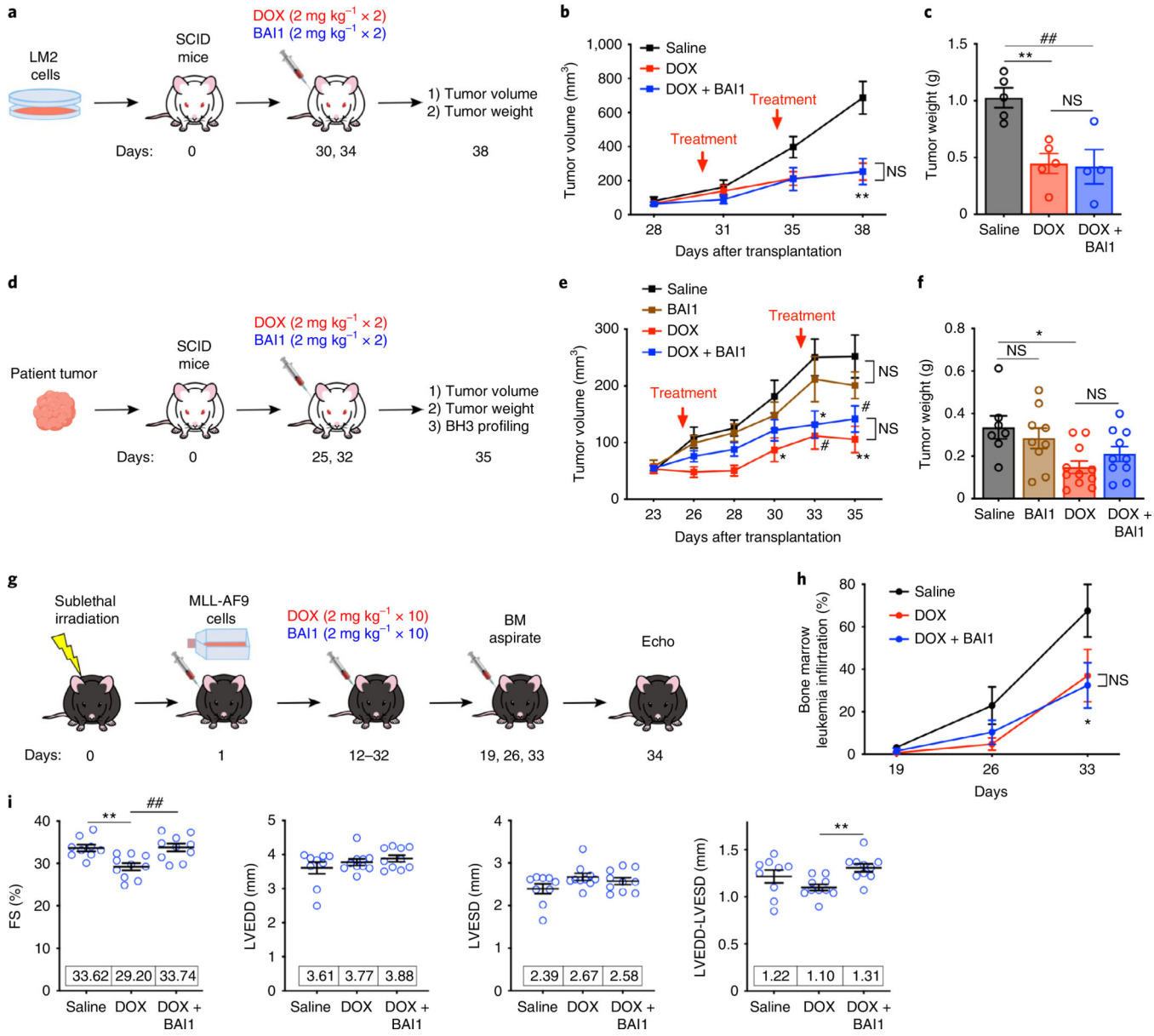

Fig. 6 |. BAI1 does not compromise the reduction of cancer burden by doxorubicin in multiple cancer models, while providing cardiac protection in the same animals.

a, Schematic of human LM2 breast cancer xenograft mouse model (recipients were 8-week-old female SCID mice). **b**, Tumor volumes at indicated times ($n = 5$ females per group). One-way ANOVA, saline versus DOX: $^{**}P = 0.0031$. **c**, Tumor weights excised postmortem 38 d after transplantation. Saline, $n = 5$; DOX, $n = 5$; DOX + BAI1, $n = 4$ females. One-way ANOVA, $^{**}P = 0.0055$; $^{\#\#}P = 0.0059$. **d**, Schematic of breast cancer PDX mouse model (recipients were 8-week-old female SCID mice). **e**, Tumor volumes at indicated times. Saline, $n = 9$; BAI1, $n = 9$; DOX, $n = 11$; DOX + BAI1, $n = 11$ females. One-way ANOVA, saline versus DOX: $^{*}P = 0.0305$, $^{\#}P = 0.0106$, $^{**}P = 0.0027$; saline versus DOX + BAI1: $^{*}P = 0.0353$, $^{\#}P = 0.0319$. **f**, Tumor weights excised postmortem 35 d after transplantation. Saline, $n = 7$; BAI1, $n = 9$; DOX, $n = 11$; DOX + BAI1, $n = 10$ females (three samples were

inadvertently not weighed). One-way ANOVA, $*P = 0.0162$. **g**, Schematic of AML allograft mouse model using mouse bone-marrow cells transfected with human MLL-AF9 oncogene (recipients were 8-week-old male C57BL/6J mice). **h**, Graphic representation of flow-cytometric analysis of leukemia burden in bone-marrow aspirates using CD45.1 (recipient) and CD45.2 (donor) antibodies ($n = 10$ males per group). One-way ANOVA, saline versus DOX: $*P = 0.0385$. **i**, Echocardiographic analysis of systolic function including FS, LVEDD, LVESD and LVEDD-LVESD of the same mice as in **g** and **h**, assessed 23 d after initiation of DOX. Saline, $n = 9$ (one mouse died of AML before echo); DOX, $n = 10$; DOX + BAI1, $n = 10$ males. Mean values are shown on the graphs. One-way ANOVA, FS, $**P = 0.0037$, $^{\#\#}P = 0.0022$; LVEDD-LVESD, $**P = 0.0091$. All data are presented as mean ± s.e.m. One-way ANOVA, NS, $P > 0.05$.

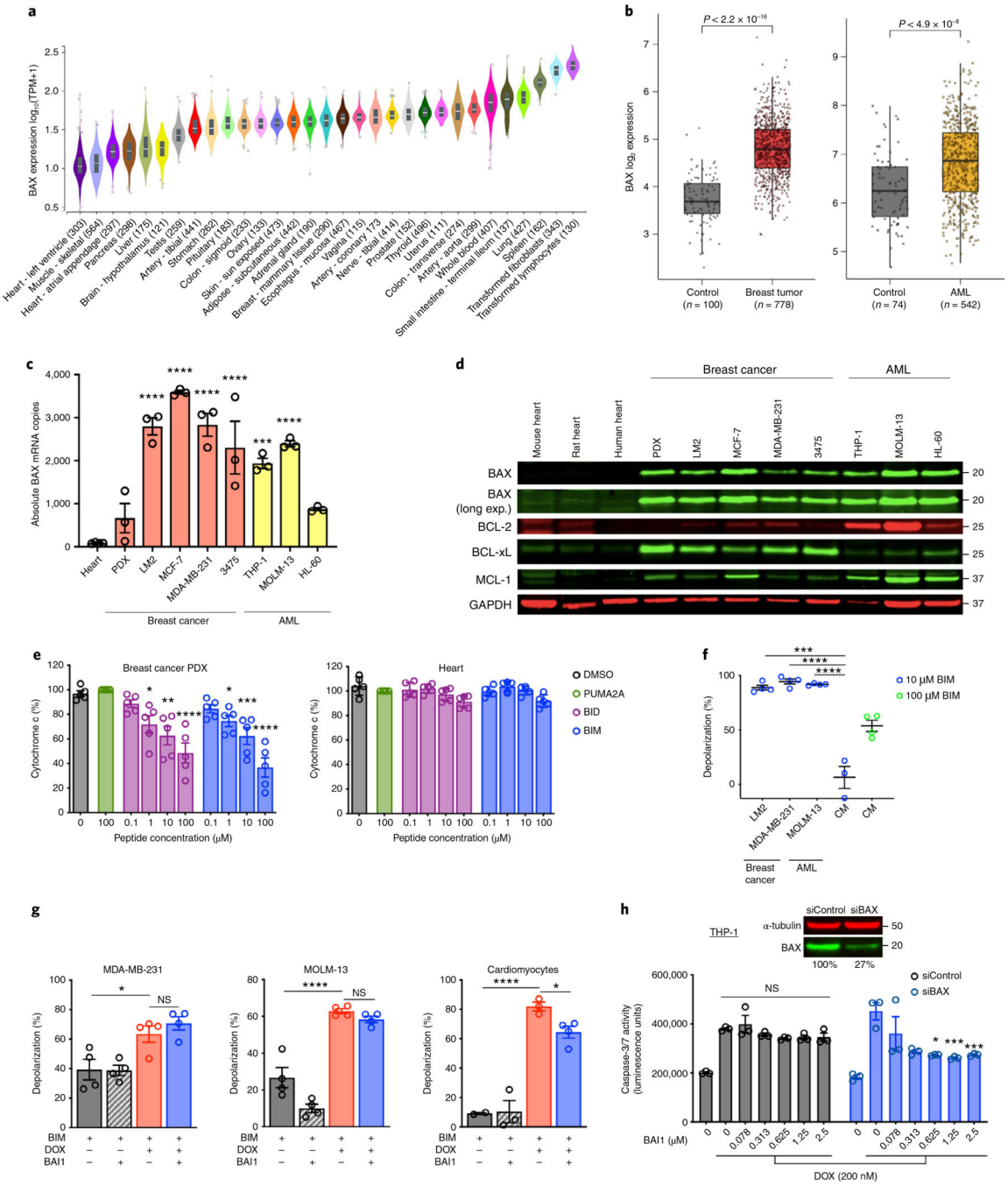

Fig. 7 |. Mechanism for BAI1 selectivity in protecting the heart against doxorubicin without compromising killing of cancer cells.

a, BAX transcript levels in various human tissues and transformed cells (Genotype-Tissue Expression project). Violin plots depict 1.5 × interquartile range (IQR), the inner box shows IQR and the central line in the box represents the median. Other observations are shown as outliers. The number of samples for each tissue is given in parentheses. **b**, BAX transcript levels in human breast cancer (The Cancer Genome Atlas) and AML (Microarray Innovations in LEukemia study) specimens compared to surrounding breast tissue and

normal blood/bone marrow respectively. Box plots depict IQR, the central line in the box shows the median and whiskers represent the minimum and maximum values. The number of samples for each tissue is given in parentheses. *P* values from two-sided Wilcoxon rank-sum test are shown on the graph. **c**,**d**, BAX is expressed at higher levels in cancers compared to heart. Absolute copy numbers of BAX transcripts in adult human heart tissue, cancers from PDX model and human breast cancer and AML cell lines assessed by qRT–PCR using a plasmid standard (**c**). Hearts, $n = 4$; others, $n = 3$. One-way ANOVA, $^{***}P = 0.0002$. BCL-2 family protein levels in adult mouse, rat and human heart tissue, cancers from PDX model and human breast cancer and AML cell lines (**d**). Data are representative of three independent experiments. **e**,**f**, Increased priming of mitochondrial death mechanisms in cancers compared to heart even under basal conditions. BH3 profiling of cells isolated from PDX cancers and adult mouse hearts stimulated with BH3 peptides from BID or BIM using flow cytometry to analyze mitochondrial cytochrome *c* retention (**e**). PUMA2A, an inactive peptide, serves as a negative control ($n = 5$ independent experiments each assessing a distinct PDX cancer and heart tissue). One-way ANOVA, compared to PUMA2A, BID, $^{*}P = 0.0130$, $^{**}P = 0.0012$; BIM, $^{*}P = 0.0102$, $^{***}P = 0.0003$. BH3 profiling of human breast cancer and AML cell lines and primary neonatal rat cardiomyocytes stimulated with BIM BH3 peptide scoring for mitochondrial depolarization with JC-1 ($n = 4, 4, 4, 3$ and 4 independent wells) (**f**). Data are representative of 2, 2, 2, 4 and 4 independent mitochondrial depolarization assays, respectively. One-way ANOVA, $^{***}P = 0.0002$. **g**, BAl1 (0.15 μM) blunts priming of mitochondrial death mechanisms in DOX-treated cardiomyocytes but not in DOX-treated cancer cells. Cancer cells and neonatal rat cardiomyocytes were stimulated with DOX and BIM to achieve 60–80% depolarization. MDA-MB-231 and MOLM-13, $n = 4$ independent wells per group (representative of two independent experiments); cardiomyocytes, $n = 2, 3, 3$ and 3 independent wells (representative of three independent experiments). One-way ANOVA, MDA-MD-231, $^{*}P = 0.0319$; cardiomyocytes: $^{*}P = 0.0261$. **h**, siRNA-mediated knockdown of BAX renders BAl1 able to reduce DOX-induced killing of cancer cells as assessed by caspase-3/7 activity ($n = 3$ independent wells per group). Data are representative of three independent experiments. One-way ANOVA, 0.625 μM, $^{*}P = 0.0203$; 1.25 μM, $^{***}P = 0.0007$; 2.5 μM, $^{***}P = 0.0004$. Data in **c**,**e**–**h** are presented as mean ± s.e.m. One-way ANOVA, $^{****}P < 0.0001$, NS, $P > 0.05$. Unprocessed images of blots are provided as source data.